Stability and Frequency Response Under Stochastic Communication Delays With Applications to Connected Cruise Control Design

Wubing B. Qin, Marcella M. Gomez, and Gábor Orosz

***Abstract*—In this paper we investigate connected cruise control in which vehicles rely on ad hoc wireless vehicle-to-vehicle communication to control their longitudinal motion. Intermittencies and packet drops in communication channels are shown to introduce stochastic delays in the feedback loops. Sufficient conditions for almost sure stability of equilibria are derived by analyzing the mean and covariance dynamics. In addition, the concept of $n\sigma$ string stability is proposed to characterize the input–output response in steady state. The stability results are summarized using stability charts in the plane of the control gains and we demonstrate that the stable regimes shrink when the sampling time or the packet drop ratio increases. The mathematical tools developed allow us to design controllers that can achieve plant stability and string stability in connected vehicle systems despite the presence of stochastically varying delays in the control loop.**

***Index Terms*—Stochastic delays, plant stability, string stability, mean dynamics, covariance dynamics.**

I. Introduction

TRAFFIC congestion [1] and road safety [2] are increasing concerns for governments due to the increasing number of vehicles. This demands for new technologies that can improve mobility, fuel economy, and safety of intelligent transportation systems. Due to the limited perception range and large reaction time of human drivers, it is difficult for drivers to maintain smooth traffic flow in a certain density range, which often leads to congestion [3]. A solution to this problem is the development of better longitudinal controllers that can attenuate fluctuations coming from the vehicles ahead, i.e., ensure string stability [4]. This can be achieved by using adaptive cruise control (ACC) [5]–[7] that utilizes a range sensor (radar, camera, or lidar) to measure the inter-vehicle distance and the relative velocity, and actuates the vehicle to maintain a velocity-dependent distance from the vehicle ahead. A limitation of ACC is that only the motion of the vehicle immediately ahead is monitored which requires a relatively large penetration of ACC vehicles to keep the traffic flow smooth [8], [9]. However, mainly due to the cost of range sensors, the penetration of ACC vehicles is still very low.

By exploiting wireless vehicle-to-vehicle (V2V) communication technologies like dedicated short range communication (DSRC) [10], [11], one may construct cooperative adaptive cruise control (CACC) [12]–[16] to overcome the perception limitation of ACC systems. The idea is to create a platoon, where each vehicle monitors the motion of the preceding vehicle by a range sensor as well as the motion of a prescribed platoon leader by V2V communication. The first experimental trial integrating ACC with wireless communication dates back to the PATH program [17] in the US, which was followed by the SARTRE project [18] and the grand cooperative driving challenge [19], [20] in Europe. CACC was shown to be able to improve traffic throughput with a high enough penetration rate [21]. However, requiring all vehicles to be equipped with range sensors and DSRC devices hinder the deployment of CACC vehicles in real traffic, while the need for a specific connectivity structure with a prescribed leader may limit modularity in the entire transportation system.

To resolve these limitations, connected cruise control (CCC) was proposed in [22] [23] which, instead of relying on a prescribed leader, exploits all the available information broadcast by multiple vehicles ahead to achieve a more accurate perception of the surrounding traffic. CCC does not require all vehicles to be equipped with range sensors and/or communication devices, but allows for human-driven vehicles in the system that may or may not broadcast their kinematic data. CCC can be used to assist the human driver, to supplement sensor based control algorithms, or to automatically control the longitudinal motion of the vehicle. Thus, one may incorporate vehicles of different levels of autonomy (from human driven to fully autonomous) in the traffic flow and improve the system-level performance while preserving modularity.

However, relying on wireless communication when controlling the motion of vehicles brings some challenges. In order to avoid channel congestion as the number of communicating vehicles increases, data cannot be exchanged too frequently. In particular, the data exchanging rate is 10 Hz for basic safety messages according to the current DSRC standards [11]. This, combined with digital control, leads to periodically varying time delays in the control loop [24], [25]. Moreover, the delay may increase further due to packet losses in a random manner

Manuscript received April 24, 2015; revised October 16, 2015, February 1, 2016, and May 4, 2016; accepted May 19, 2016. Date of publication July 18, 2016; date of current version February 1, 2017. This work was supported by the U.S. National Science Foundation under Grant 1300319. The Associate Editor for this paper was M. Chowdhury.

W. B. Qin and G. Orosz are with the Department of Mechanical Engineering, University of Michigan, Ann Arbor, MI 48109 USA (e-mail: wubing@umich.edu; orosz@umich.edu).

M. M. Gomez is with the Department of Electrical Engineering and Computer Science, University of California, Berkeley, CA 94720 USA (e-mail: mmgomez@berkeley.edu).

Color versions of one or more of the figures in this paper are available online at http://ieeexplore.ieee.org.

Digital Object Identifier 10.1109/TITS.2016.2574246

[26]. In [27] digital effects were taken into account and necessary conditions of stability were provided based on the mean dynamics while assuming delays of equal probability. (Here, the mean dynamics refer to the time evolution of the expected value of the state.) In [28] a continuous time approximation was taken and sufficient conditions of stability were provided while taking into account the uncertainties in the delays. However, the stochastic processes describing the delay variations have not yet been incorporated in the control loop and string stability has not yet been characterized in the presence of stochastically varying time delays. In this paper we target these challenging problems.

Evaluating the response of dynamic systems subject to stochastic delay variations depends on how convergence and stability are defined. In engineering applications we are particularly interested in conditions that ensure almost sure stability since it allows for the design of controllers that ensure convergence of almost all trajectories despite having stochastic delay variations in the control loop. While Lyapunov stability theorems are often used to obtain stability conditions for continuous and discrete time systems [29]–[32], these typically lead to very conservative stability conditions. However, for discrete-time linear systems with stochastic delays the second moment dynamics may be analyzed [33]–[36] to ensure almost sure stability. Here we consider this approach to analyze the stability of the equilibrium, often referred to as plant stability, in connected vehicle systems.

On the other hand, no mathematical tools exist that can ensure the desired frequency response under stochastic delay variations. This is needed to evaluate disturbance attenuation about the equilibrium and often referred to as string stability connected vehicle systems. To handle this problem we analyze the covariance dynamics and establish the concept of $n\sigma$ *string stability*. This allows us to design controllers that can ensure attenuation of perturbations despite stochastically varying time delays. We demonstrate the developed mathematical techniques on a simplified vehicle model regulated by a simple controller while using a Bernoulli process to describe the delay variation. Nevertheless, our method can be applied when considering higher fidelity vehicle models, more sophisticated controllers, and different stochastic processes.

The layout of this paper is as follows. Some preliminaries are provided in Section II regarding the Kronecker product formulation and definitions for stability of stochastic systems. In Section III we provide a dynamic model to describe stochastic delay variations and present the connected cruise controller used in the rest of the paper. In Section IV we assume a simplified delay evolution and use the dynamics of the mean to derive necessary conditions of plant stability and string stability. We also determine the covariance dynamics and derive sufficient conditions for plant stability and $n\sigma$ string stability. The stability results are presented in a concise manner using stability diagrams on the plane of gain parameters for different values of packet delivery ratio and sampling time. In Section V we present the results subject to the true delay dynamics while in Section VI numerical simulations are used to demonstrate the implications of the stability charts at the nonlinear level. Finally, conclusions are drawn and future research directions are laid out in Section VII.

II. Preliminaries

In this section we define the notation and state some theorems regarding stability of stochastic systems used in the rest of the paper.

A. Kronecker Product and $\overline{vec}$ Operator

In this paper, we use the Kronecker product and vectorization of matrices when expressing the dynamics of the k-th moment of vector-valued quantities. We recall the following definitions and theorems from [37].

Definition 1: Let $h_i \in \mathbb{R}^n$ denote the i-th column of matrix $\mathbf{H} \in \mathbb{R}^{n\times m}$, i.e., $\mathbf{H} = [h_1 \ h_2 \ \dots \ h_m]$. The vector operator defined by

$$\overline{\text{vec}}(\mathbf{H}) = \begin{bmatrix} h_1^T & h_2^T & \dots & h_m^T \end{bmatrix}^T \in \mathbb{R}^{mn} \tag{1}$$

inserts the columns of the matrix below each other.

Theorem 1: For matrices $\mathbf{A} \in \mathbb{R}^{m\times n}$, $\mathbf{B} \in \mathbb{R}^{n\times l}$, $\mathbf{C} \in \mathbb{R}^{p\times q}$, and $\mathbf{D} \in \mathbb{R}^{q\times r}$, we have

$$(\mathbf{AB}) \otimes (\mathbf{CD}) = (\mathbf{A} \otimes \mathbf{C})(\mathbf{B} \otimes \mathbf{D}) \tag{2}$$

where $\otimes$ denotes Kronecker product.

Theorem 2: For any three matrices $\mathbf{A}$, $\mathbf{B}$ and $\mathbf{C}$ for which the matrix product $\mathbf{ABC}$ is defined, we can write

$$\overline{\text{vec}}(\mathbf{ABC}) = (\mathbf{C}^T \otimes \mathbf{A})\overline{\text{vec}}(\mathbf{B}). \tag{3}$$

Definition 2: For a random variable $X \in \mathbb{R}^n$, the mean and second moment are defined as $\mathbb{E}[X] \in \mathbb{R}^n$ and $\mathbb{E}[XX^T] \in \mathbb{R}^{n\times n}$, where $\mathbb{E}$ denotes the expected value. Similarly, the second central moment or covariance matrix is defined as $\mathbb{E}[(X - \mathbb{E}[X])(X - \mathbb{E}[X])^T] \in \mathbb{R}^{n\times n}$. Using Definition 1 and Theorem 2, one may show that

$$\begin{aligned} &\overline{\text{vec}}\left(\mathbb{E}[XX^T]\right) = \mathbb{E}[X \otimes X] \\ &\overline{\text{vec}}\left(\mathbb{E}\left[(X - \mathbb{E}[X])\,(X - \mathbb{E}[X])^T\right]\right) \\ &\qquad = \mathbb{E}\left[(X - \mathbb{E}[X]) \otimes (X - \mathbb{E}[X])\right]. \end{aligned} \tag{4}$$

B. Stochastic Stability

There are many different types of stochastic stability defined in the literature, and their relationships and properties can be found in [38]–[42]. Here we are only interested in certain notions of stochastic stability and we will develop theorems using the following definitions.

Definition 3: A random sequence $\{X(k) \in \mathbb{R}^n\}_{k=0}^{+\infty}$ converges to X^* almost surely if

$$\mathbb{P}\left[\lim_{k\to\infty} X(k) = X^*\right] = 1. \tag{5}$$

If sequences generated by a stochastic dynamical system converge to X^* almost surely, then the solution $X(k) \equiv X^*$ is almost surely asymptotically stable.

Note that almost sure convergence is also called convergence with probability one.

Definition 4: A random sequence $\{X(k) \in \mathbb{R}^n\}_{k=0}^{+\infty}$ converges to X^* in the p-th moment if

$$\lim_{k\to\infty} \mathbb{E}\left[\underbrace{(X(k)-X^*)\otimes\cdots\otimes(X(k)-X^*)}_{p \text{ times}}\right] = 0. \quad (6)$$

If sequences generated by a stochastic dynamical system converge to X^* in the p-th moment, then the solution $X(k) \equiv X^*$ is asymptotically stable in the p-th moment.

It can be shown that stability in the second moment implies stability in the first moment (often called mean stability). In general there is no relationship between almost sure stability and moment stability but based on [43] (Theorem 8 in Chapter 8) we can state the following theorem.

Theorem 3: For the discrete-time linear stochastic system $X(k+1) = \mathbf{A}(k)X(k)$, where $\mathbf{A}(k)$ are mutually independently identically distributed matrices, asymptotic stability in the second moment implies almost sure asymptotic stability.

In the following sections we will investigate the covariance dynamics so we state the following theorem.

Theorem 4: For a discrete-time stochastic system, the second moment $\mathbb{E}[X(k) \otimes X(k)]$ is asymptotically stable if and only if the first moment $\mathbb{E}[X(k)]$ and the covariance $\mathbb{E}[(X(k) - \mathbb{E}[X(k)]) \otimes (X(k) - \mathbb{E}[X(k)])]$ are asymptotically stable.

The proof can be constructed by exploiting the relationship between the mean, the second moment and the covariance; see Definition 2. Also, using the definitions and theorems above we can state the following theorem.

Theorem 5: For the discrete-time linear stochastic system $X(k+1) = \mathbf{A}(k)X(k)$, where $\mathbf{A}(k)$ are mutually independently identically distributed matrices, if the system is stable in the first moment, then asymptotic stability in covariance implies asymptotic stability in the second moment and almost sure asymptotic stability.

III. Connected Cruise Control With Stochastic Delays

In this section we present our connected cruise control design while incorporating stochastic delay variations in the communication links. Fig. 1 shows a vehicle chain where each vehicle is using the information received from the car immediately ahead. This can be viewed as the concatenation of leader-follower pairs. We consider a nonlinear controller that acts on the inter-vehicle distance h (called distance headway), the leader's velocity v_{L}, and the vehicle's own velocity v. We assume that the distance headway can be calculated from GPS coordinates of the vehicle with adequate accuracy. For simplicity, we assume that the clocks of the leader and follower are synchronized. This assumption may not hold in real DSRC networks and may lead to a change of the time delays. However, as will be shown below, delays vary more due to packet drops than due to asynchrony of the clocks, so we focus on the former effects in this paper.

We assume that the leader broadcasts its kinematic information intermittently with the sampling time Δt, which results in the time mesh $t_k = k\Delta t$ for $k = 0, 1, 2, \ldots$; see Fig. 2(a). According to the IEEE802.11p protocol, the sender is unaware whether a broadcasted packet has been successfully delivered

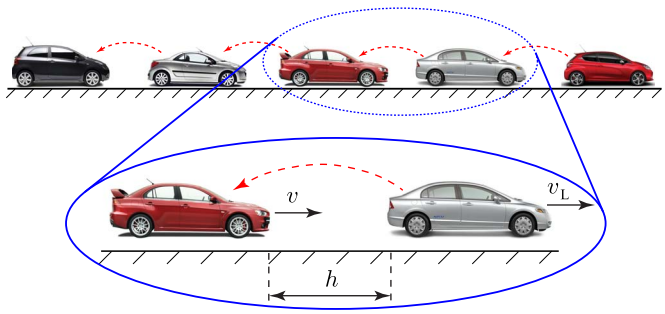

Fig. 1. Top row shows a chain of vehicles equipped with wireless communication on a single lane, which is the concatenation of leader–follower pairs zoomed at the bottom. Dashed arrows indicate V2V links between vehicles.

and no packets are resent. We assume that at time instant t_k, previous $\tau(k) - 1$ packets have been dropped consecutively. Thus, the last packet successfully received was at time instant $t_{k-\tau(k)}$. The controller outputs a command based on this information at $t_{k-\tau(k)+1}$ that is kept constant until t_{k+1} using a zero-order hold (ZOH), since no new packet is delivered successfully until t_k; see Fig. 2(b). We assume that the packet drop dynamics is governed by a stochastic process, that is, the digitally controlled system is forced by piecewise constant inputs of stochastically varying length.

The methods developed below can be applied to any car-following model subject to digital control under any (stationary) stochastic process describing the packet drop dynamics. However, in order to make the problem tractable we assume that the parameters of the stochastic process (e.g., packet delivery ratio) are constant (or vary much slower than the vehicle dynamics). In reality such assumptions may not hold as the state of vehicles (speed and distance) as well as the environment (geography, buildings, weather) may influence the packet drop dynamics. Studying such effects requires real data [44] and is left for future research.

To further simplify the matter we model the packet drop dynamics using Bernoulli trials [45]. That is, the time evolution of $\tau(k)$ can be formulated as

$$\tau(k+1) = \begin{cases} 1, & \text{if a packet is received} \\ & \text{during } [t_k,\ t_{k+1}) \\ \tau(k)+1, & \text{otherwise.} \end{cases} \quad (7)$$

According to the Bernoulli process we assume that the successful delivery of a packet is independent of whether other packets are delivered and we denote the packet delivery ratio by p. To avoid infinitely long delays, we also assume that the maximum of $\tau(k)$ is N, i.e., $\tau(k+1) = 1$ if $\tau(k) = N$. This yields the probability density function (PDF)

$$f_{\tau(k)}(\xi) = \sum_{r=1}^{\infty} w_r \delta(\xi - r) \quad (8)$$

where $\delta(*)$ denotes the Dirac delta function, and the $w_r - s$ are defined as

$$w_r = \begin{cases} p(1-p)^{r-1} & \text{if} \quad r = 1, \ldots, N-1 \\ 1 - \sum_{i=1}^{N-1} w_i = (1-p)^{N-1} & \text{if} \quad r = N \\ 0 & \text{if} \quad r > N. \end{cases} \quad (9)$$

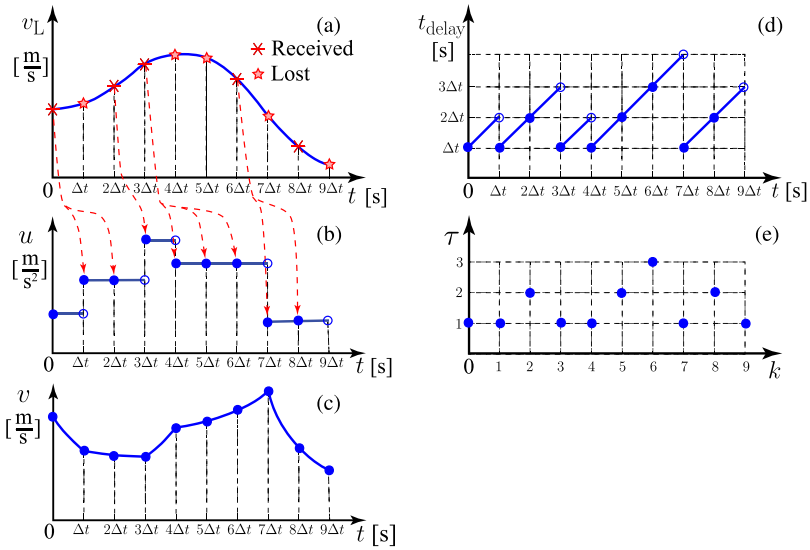

Fig. 2. (a) Leader's velocity is transmitted every Δt time, but packets may be dropped as indicated. (b) Controller output while using a zero-order hold based on the newest received information. (c) Follower's velocity based on controller in panel (b). (d) Time delay variations in the continuous-time system (10), (11). (e) Corresponding delays in the discrete-time system (15).

We remark that N is chosen such that $\sum_{r=1}^{N-1} w_r \geq \hat{p}$ holds where $\hat{p}$ is the critical cumulative delivery ratio. For example, considering $p = 0.6$ and setting $\hat{p} = 0.99$, the maximum value is $N = 6$. These assumptions are confirmed by the experimental results in [46].

Notice that even though the probability distribution of $\tau(k+1)$ is not independent of $\tau(k)$, i.e., (7) describes a non-Markovian stochastic process, the probability distributions are still identically geometrically distributed for each discrete time k. In Section IV we will simplify the analysis by using the distribution (8), (9) while substituting the non-Markovian stochastic process (7) with a Markovian one. In Section V we will return to the original problem and demonstrate that the mathematical tools developed can be extended to a general stationary stochastic process. Finally, we emphasize that while the packet drop dynamics are described in discrete time due to the intermittent communication, the dynamics of the vehicles still evolve in continuous time; see Fig. 2(c). The corresponding effective delay increases from $\tau(k)\Delta t$ to $(\tau(k)+1)\Delta t$ linearly during each sampling interval, as shown in Fig. 2(d).

As mentioned above, vehicle models of different levels of fidelity and controllers of different levels of complexity may be considered. For simplicity we consider zero inclination and omit the rolling resistance and air drag effects in the physics-based model [23], which leads to the simplified dynamics

$$\begin{aligned} \dot{h}(t) =& v_{\mathrm{L}}(t) - v(t) \\ \dot{v}(t) =& u(t_{k-\tau(k)}) \end{aligned} \tag{10}$$

for $t \in [t_k, t_{k+1})$. Moreover, we choose a simple nonlinear controller

$$u(t) = K_p \left(V\left(h(t)\right) - v(t)\right) + K_v \left(W\left(v_L(t)\right) - v(t)\right) \tag{11}$$

that was constucted in [47]. This is a generalization of the linear controller that is widely used in the literature [12], [15], [48].

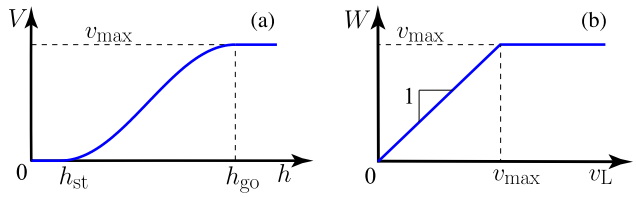

Fig. 3. (a) Range policy function (12). (b) Saturation function (13).

The range policy $V(h)$ gives the desired velocity as a function of the distance headway h, and it is

- continuous and monotonously increasing (the more sparse traffic is, the faster the vehicle intends to run);
- zero for $h \leq h_{\mathrm{st}}$ (vehicles intend to stop within a safety distance);
- maximal for $h \geq h_{\mathrm{go}}$ (vehicles want to travel fast in sparse traffic—often called free flow).

Here we choose the continuously differentiable range policy

$$V(h) = \begin{cases} 0 & \text{if} \quad h \leq h_{\mathrm{st}} \\ \frac{v_{\max}}{2}\left(1 - \cos\left(\pi \frac{h - h_{\mathrm{st}}}{h_{\mathrm{go}} - h_{\mathrm{st}}}\right)\right) & \text{if} \quad h_{\mathrm{st}} < h < h_{\mathrm{go}} \\ v_{\max} & \text{if} \quad h \geq h_{\mathrm{go}} \end{cases} \tag{12}$$

shown in Fig. 3(a). Moreover, the saturation function $W(v_L)$ describes the switching between CCC mode ($v_L \leq v_{\max}$) and normal cruise control mode ($v_L > v_{\max}$) such that

$$W(v_L) = \begin{cases} v_L & \text{if} \quad v_L \leq v_{\max} \\ v_{\max} & \text{if} \quad v_L > v_{\max} \end{cases} \tag{13}$$

see Fig. 3(b).

For $v_L \leq v_{\max}$ (CCC mode), system (10), (11) possesses the equilibrium

$$v_L^* = v^* = V(h^*). \tag{14}$$

Our goal is to design the control gains K_p, K_v to ensure that the system can reach this equilibrium (i.e., plant stability is satisfied) and also attenuate perturbations introduced by the leader (i.e., string stability holds) in the presence of stochastic communication delays.

A. Discretization and Linearization

Solving the differential equation (10), (11) with input $v_L(t)$ along the time interval $t \in [t_k, t_{k+1})$, one may derive the discrete-time nonlinear map. Following the process in Appendix A, we obtain:

$$\begin{aligned}\begin{bmatrix} h(t_{k+1}) \\ v(t_{k+1}) \end{bmatrix} &= \begin{bmatrix} 1 & -\Delta t \\ 0 & 1 \end{bmatrix} \begin{bmatrix} h(t_k) \\ v(t_k) \end{bmatrix} + \begin{bmatrix} \int_{t_k}^{t_{k+1}} v_L(t)\mathrm{d}t \\ 0 \end{bmatrix} \\ &+ \begin{bmatrix} 0 & \frac{1}{2}\Delta t^2(K_p + K_v) \\ 0 & -\Delta t(K_p + K_v) \end{bmatrix} \begin{bmatrix} h\left(t_{k-\tau(k)}\right) \\ v\left(t_{k-\tau(k)}\right) \end{bmatrix} \\ &+ \begin{bmatrix} -\frac{1}{2}\Delta t^2 K_p \\ \Delta t K_p \end{bmatrix} V\left(h\left(t_{k-\tau(k)}\right)\right) \\ &+ \begin{bmatrix} -\frac{1}{2}\Delta t^2 K_v \\ \Delta t K_v \end{bmatrix} W\left(v_L\left(t_{k-\tau(k)}\right)\right) \end{aligned} \tag{15}$$

where $\tau(k)$ plays the role of a discrete stochastic delay; see Fig. 2(e). Note that (15) is a nonlinear stochastic difference equation since the stochasticity in $\tau(k)$ leads to stochasticity in $h(k)$ and $v(k)$. In order to characterize the stochastic dynamics one may derive deterministic equations that describe the time evolution of the moments. However, for a nonlinear system the time evolution of the lower moments are influenced by the higher moments and "moment closure" may not be achieved in general. To simplify the matter, we first linearize the stochastic system (15) and then derive the equations describing time evolution of the first and second moments. In this case the dynamics of the first moment is self contained while the dynamics of the second moment is driven by that of the first moment.

In order to linearize (15) about the equilibrium (14), we define the perturbations $v_L(t) = v_L^* + \tilde{v}_L(t)$, $\tilde{h}(t) = h(t) - h^*$, $\tilde{v}(t) = v(t) - v^*$. Moreover, Fourier's theory states that periodic signals can be represented as a countable sum of sines and cosines, which can also be extended to absolutely integrable non-periodic signals using Fourier transform. Henceforth, we assume sinusoidal variations of the leader's velocity, i.e.,

$$v_L(t) = v_L^* + v_L^{\text{amp}} \sin(\omega\, t) \Longrightarrow \tilde{v}_L(t) = v_L^{\text{amp}} \sin(\omega\, t) \tag{16}$$

and $v_L(t) < v_{\max}$.

By defining the state, the input and the output as

$$x(k) = \begin{bmatrix} \tilde{h}(t_k) \\ \tilde{v}(t_k) \end{bmatrix},\ u(k) = \begin{bmatrix} \tilde{v}_L(t_k) \\ \tilde{v}_L^{\perp}(t_k) \end{bmatrix},\ y(k) = \tilde{v}(t_k) \tag{17}$$

where

$$\tilde{v}_L^{\perp}(t) = v_L^{\text{amp}} \cos(\omega t) \tag{18}$$

the linearization of (15) becomes

$$\begin{aligned} x(k+1) &= \boldsymbol{a}\, x(k) + \boldsymbol{a}_\tau\, x\left(k - \tau(k)\right) \\ &\quad + \boldsymbol{b}\, u(k) + \boldsymbol{b}_\tau\, u\left(k - \tau(k)\right) \\ y(k) &= \boldsymbol{c}\, x(k) \end{aligned} \tag{19}$$

with matrices

$$\begin{aligned} \boldsymbol{a} &= \begin{bmatrix} 1 & -\Delta t \\ 0 & 1 \end{bmatrix}, \quad \boldsymbol{b} = \begin{bmatrix} \alpha_1 & \alpha_2 \\ 0 & 0 \end{bmatrix} \\ \boldsymbol{a}_\tau &= \begin{bmatrix} -\frac{1}{2}\Delta t^2 K_p N_* & \frac{1}{2}\Delta t^2(K_p + K_v) \\ \Delta t K_p N_* & -\Delta t(K_p + K_v) \end{bmatrix} \\ \boldsymbol{b}_\tau &= \begin{bmatrix} -\frac{1}{2}\Delta t^2 K_v & 0 \\ \Delta t K_v & 0 \end{bmatrix}, \quad \boldsymbol{c} = \begin{bmatrix} 0 & 1 \end{bmatrix} \end{aligned} \tag{20}$$

where

$$\begin{aligned} \alpha_1 &= \frac{\sin(\omega\Delta t)}{\omega}, \quad \alpha_2 = \frac{1 - \cos(\omega\Delta t)}{\omega} \\ N_* &= V'(h^*) = V'\left(V^{-1}(v^*)\right) \\ &= \begin{cases} \frac{\pi\sqrt{v^*(v_{\max} - v^*)}}{h_{\text{go}} - h_{\text{st}}} & \text{if} \quad h_{\text{st}} < h < h_{\text{go}} \\ 0 & \text{elsewhere} \end{cases} \end{aligned} \tag{21}$$

cf. (12). Notice that the scalar sinusoidal input (16) that drives the continuous-time system (10), (11) results in the vector-valued input (17) for the discrete-time system (19), although the two inputs are not independent. Also, notice that the input satisfies

$$u(k - r) = \mathbf{R}^r\, u(k) \tag{22}$$

where

$$\mathbf{R} = \begin{bmatrix} \cos(\omega\Delta t) & -\sin(\omega\Delta t) \\ \sin(\omega\Delta t) & \cos(\omega\Delta t) \end{bmatrix}. \tag{23}$$

Defining the augmented state, the input and the output as

$$\begin{aligned} X(k) &= \begin{bmatrix} x(k) \\ x(k-1) \\ \vdots \\ x(k-N) \end{bmatrix} \in \mathbb{R}^{2(N+1)} \\ U(k) &= u(k) \in \mathbb{R}^2, \quad Y(k) = y(k) \in \mathbb{R} \end{aligned} \tag{24}$$

respectively, (19) can be written as

$$\begin{aligned} X(k+1) &= \mathbf{A}_{\tau(k)}\, X(k) + \mathbf{B}_{\tau(k)}\, U(k) \\ Y(k) &= \mathbf{C}\, X(k) \end{aligned} \tag{25}$$

where $\mathbf{A}_{\tau(k)} \in \mathbb{R}^{2(N+1)\times 2(N+1)}$ and $\mathbf{B}_{\tau(k)} \in \mathbb{R}^{2(N+1)\times 2}$ can take the values

$$\begin{aligned} \mathbf{A}_r &= \begin{bmatrix} \boldsymbol{a} & \delta_{1r}\, \boldsymbol{a}_\tau & \delta_{2r}\, \boldsymbol{a}_\tau & \cdots & \delta_{Nr}\, \boldsymbol{a}_\tau \\ \mathbf{I} & \mathbf{0} & \mathbf{0} & \cdots & \mathbf{0} \\ \mathbf{0} & \mathbf{I} & \mathbf{0} & \cdots & \mathbf{0} \\ \vdots & & \ddots & \ddots & \vdots \\ \mathbf{0} & \cdots & \mathbf{0} & \mathbf{I} & \mathbf{0} \end{bmatrix} \\ \mathbf{B}_r &= \begin{bmatrix} \boldsymbol{b} + \boldsymbol{b}_\tau\, \mathbf{R}^r \\ \mathbf{0} \\ \vdots \\ \mathbf{0} \end{bmatrix} \end{aligned} \tag{26}$$

for $r = 1, \ldots, N$; cf. (20). Here, δ_{sr} denotes the Kronecker delta, while $\mathbf{I} \in \mathbb{R}^{2\times 2}$ and $0 \in \mathbb{R}^{2\times 2}$ denote the identity and zero matrices, respectively. Also we have

$$\mathbf{C} = \begin{bmatrix} \boldsymbol{c} & 0 & \cdots & 0 \end{bmatrix} \in \mathbb{R}^{1\times 2(N+1)}. \tag{27}$$

IV. Mean and Covariance Dynamics—IID Approximation

In order to find the stability condition, the mean, the second moment, and the covariance dynamics shall be derived. In (25), $\mathbf{A}_{\tau(k)}$ depends on $\mathbf{A}_{\tau(k-1)}$ according to (7), which is also the case for $\mathbf{B}_{\tau(k)}$ and $\mathbf{B}_{\tau(k-1)}$, implying that (25) describes a non-Markovian stochastic process. In order to simplify the analysis, instead of using (7) we assume that $\tau(k)$-s are independently identically distributed (IID) while still keeping the probability density function (8), (9) which results in Markovian dynamics. In Section V, we will demonstrate that this gives a good approximation of the true stability.

With the IID assumption of $\tau(k)$, one can obtain the joint PDF of $\mathbf{A}_{\tau(k)}$ and $\mathbf{B}_{\tau(k)}$ from (8) as

$$f_{\mathbf{A}_{\tau(k)},\mathbf{B}_{\tau(k)}}(\mathbf{A},\mathbf{B}) = \sum_{r=1}^{\infty}\sum_{s=1}^{\infty} w_r\delta_{rs}\,\delta(\mathbf{A}-\mathbf{A}_r)\delta(\mathbf{B}-\mathbf{B}_s). \tag{28}$$

From this, the marginal PDF-s of $\mathbf{A}_{\tau(k)}$ and $\mathbf{B}_{\tau(k)}$ can be obtained as

$$\begin{aligned} f_{\mathbf{A}_{\tau(k)}}(\mathbf{A}) &= \sum_{r=1}^{\infty} w_r\delta(\mathbf{A}-\mathbf{A}_r) \\ f_{\mathbf{B}_{\tau(k)}}(\mathbf{B}) &= \sum_{r=1}^{\infty} w_r\delta(\mathbf{B}-\mathbf{B}_r) \end{aligned} \tag{29}$$

respectively. Notice that $\mathbf{A}_{\tau(k)}$ and $X(k)$ are mutually independent, which is also the case for $\mathbf{B}_{\tau(k)}$ and $X(k)$.

Let us define the deterministic variables

$$\bar{X}(k) = \mathbb{E}[X(k)] \in \mathbb{R}^{2(N+1)}, \bar{Y}(k) = \mathbb{E}[Y(k)] \in \mathbb{R}. \tag{30}$$

By taking expectations of both sides in (25) and using independency between state variables and the PDF-s (29), one can derive the mean dynamics

$$\begin{aligned} \bar{X}(k+1) &= \bar{\mathbf{A}}\,\bar{X}(k) + \bar{\mathbf{B}}\,U(k) \\ \bar{Y}(k) &= \bar{\mathbf{C}}\,\bar{X}(k) \end{aligned} \tag{31}$$

where the matrices are

$$\bar{\mathbf{A}} = \sum_{r=1}^{N} w_r\mathbf{A}_r, \quad \bar{\mathbf{B}} = \sum_{r=1}^{N} w_r\mathbf{B}_r, \quad \bar{\mathbf{C}} = \mathbf{C}. \tag{32}$$

Notice that the mean dynamics (30)–(32) can be rewritten for the mean of the variables used in (19) as a deterministic distributed delay difference equation with delay distribution (8), i.e.,

$$\begin{aligned} \bar{x}(k+1) =& \boldsymbol{a}\,\bar{x}(k) + \sum_{r=1}^{N} w_r\boldsymbol{a}_r\,\bar{x}(k-r) \\ &+ \boldsymbol{b}\,u(k) + \sum_{r=1}^{N} w_r\boldsymbol{b}_r\,u(k-r) \\ \bar{y}(k) =& \boldsymbol{c}\,\bar{x}(k) \end{aligned} \tag{33}$$

where

$$\bar{x}(k) = \mathbb{E}[x(k)] \in \mathbb{R}^2, \bar{y}(k) = \mathbb{E}[y(k)] \in \mathbb{R}. \tag{34}$$

Let us define the second moments

$$\begin{aligned} \hat{\bar{X}}(k) &= \mathbb{E}[X(k)\otimes X(k)] \in \mathbb{R}^{4(N+1)^2} \\ \hat{\bar{Y}}(k) &= \mathbb{E}[Y(k)\otimes Y(k)] \in \mathbb{R}. \end{aligned} \tag{35}$$

By taking expectations and using independency between variables and the PDF-s (28), (29), one can obtain the second moment dynamics

$$\begin{aligned} \hat{\bar{X}}(k+1) =& \left(\sum_{r=1}^{N} w_r\mathbf{A}_r\otimes\mathbf{A}_r\right)\hat{\bar{X}}(k) \\ &+ \left(\sum_{r=1}^{N} w_r\mathbf{A}_r\otimes\mathbf{B}_r\right)\left(\bar{X}(k)\otimes U(k)\right) \\ &+ \left(\sum_{r=1}^{N} w_r\mathbf{B}_r\otimes\mathbf{A}_r\right)\left(U(k)\otimes\bar{X}(k)\right) \\ &+ \left(\sum_{r=1}^{N} w_r\mathbf{B}_r\otimes\mathbf{B}_r\right)(U(k)\otimes U(k)) \\ \hat{\bar{Y}}(k) =& (\mathbf{C}\otimes\mathbf{C})\,\hat{\bar{X}}(k). \end{aligned} \tag{36}$$

Moreover, the covariance can be defined as

$$\begin{aligned} \bar{\bar{X}}(k) &= \mathbb{E}\left[\left(X(k)-\bar{X}(k)\right)\otimes\left(X(k)-\bar{X}(k)\right)\right] \in \mathbb{R}^{4(N+1)^2} \\ \bar{\bar{Y}}(k) &= \mathbb{E}\left[\left(Y(k)-\bar{Y}(k)\right)\otimes\left(Y(k)-\bar{Y}(k)\right)\right] \in \mathbb{R} \end{aligned} \tag{37}$$

and it can be shown that

$$\begin{aligned} \bar{\bar{X}}(k) &= \mathbb{E}[X(k)\otimes X(k)] - \bar{X}(k)\otimes\bar{X}(k) \\ \bar{\bar{Y}}(k) &= \mathbb{E}[Y(k)\otimes Y(k)] - \bar{Y}(k)\otimes\bar{Y}(k). \end{aligned} \tag{38}$$

Thus, using (31) and (36), one can obtain the covariance dynamics

$$\begin{aligned} \bar{\bar{X}}(k+1) =& \bar{\bar{\mathbf{A}}}\bar{\bar{X}}(k) \\ &+ \bar{\bar{\mathbf{H}}}_1\left(\bar{X}(k)\otimes U(k)\right) + \bar{\bar{\mathbf{H}}}_2\left(U(k)\otimes\bar{X}(k)\right) \\ &+ \bar{\bar{\mathbf{H}}}_3\left(U(k)\otimes U(k)\right) + \bar{\bar{\mathbf{H}}}_4\left(\bar{X}(k)\otimes\bar{X}(k)\right) \\ \bar{\bar{Y}}(k) =& \bar{\bar{\mathbf{C}}}\bar{\bar{X}}(k) \end{aligned} \tag{39}$$

where

$$\bar{\bar{\mathbf{A}}} = \sum_{r=1}^{N} w_r \mathbf{A}_r \otimes \mathbf{A}_r$$

$$\bar{\bar{\mathbf{H}}}_1 = \sum_{r=1}^{N} w_r \mathbf{A}_r \otimes \mathbf{B}_r - \bar{\mathbf{A}} \otimes \bar{\mathbf{B}}$$

$$\bar{\bar{\mathbf{H}}}_2 = \sum_{r=1}^{N} w_r \mathbf{B}_r \otimes \mathbf{A}_r - \bar{\mathbf{B}} \otimes \bar{\mathbf{A}}$$

$$\bar{\bar{\mathbf{H}}}_3 = \sum_{r=1}^{N} w_r \mathbf{B}_r \otimes \mathbf{B}_r - \bar{\mathbf{B}} \otimes \bar{\mathbf{B}}$$

$$\bar{\bar{\mathbf{H}}}_4 = \sum_{r=1}^{N} w_r \mathbf{A}_r \otimes \mathbf{A}_r - \bar{\mathbf{A}} \otimes \bar{\mathbf{A}}$$

$$\bar{\bar{\mathbf{C}}} = \mathbf{C} \otimes \mathbf{C} \tag{40}$$

cf. (31), (32). The time evolutions of the mean and the covariance are described by the nonlinear system (31), (39) so that (39) is driven by (31).

A. Plant Stability

Plant stability is achieved when the follower's velocity asymptotically approaches a constant reference velocity dictated by the leader. In other words, the system is plant unstable if the follower's velocity diverges in an oscillatory or non-oscillatory way when the leader's velocity is set to be constant. To test plant stability, we set $v_L^{\text{amp}} = 0$ in (16) and (18) or $u(k) = 0$ in (17). First, we investigate the plant stability of the mean dynamics (31), which means the mean value of the follower's velocity approaches the leader's velocity. Then we study the plant stability of the second moment dynamics (36) [or equivalently the covariance dynamics (39)], which means that the variance of the follower's velocity converges to zero. The plant stability for the mean dynamics is a necessary condition for the plant stability of the stochastic system (25). On the other hand, the plant stability of the second moment dynamics (36) [or the covariance dynamics (39)] provides a sufficient condition for the (almost sure) plant stability of the stochastic system (25) according to Theorem 5.

For plant stability of the mean dynamics $\bar{X}(k+1) = \bar{\mathbf{A}}\bar{X}(k)$ (cf. (31) with $U(k) = 0$), all the eigenvalues $z \in \mathbb{C}$ of the matrix $\bar{\mathbf{A}}$ must lie within the unit circle in the complex plane. These eigenvalues are given by the characteristic equation

$$\det(z\,\bar{\mathbf{I}} - \bar{\mathbf{A}}) = 0 \tag{41}$$

where $\bar{\mathbf{I}} \in \mathbb{R}^{2(N+1)\times 2(N+1)}$ is the identity matrix. There are three different ways in which the system can lose stability [49]: (i) One real eigenvalue crosses the unit circle at 1, which corresponds to non-oscillatory divergence of the solution; (ii) One real eigenvalue crosses the unit circle at -1, which corresponds to oscillatory divergence of the solutions with (the highest possible) angular frequency $\pi/\Delta t$ allowed by the discrete time steps; (iii) A pair of complex conjugate eigenvalues crosses the unit circle at $\mathrm{e}^{\pm \mathrm{j}\theta}$, $\theta \in (0, \pi)$, which corresponds to oscillatory divergence of the solutions with angular frequency $\theta/\Delta t \in (0, \pi/\Delta t)$. By substituting the critical eigenvalue(s) into the characteristic equation (41), one can obtain the stability boundaries represented in the parameter space $(K_p, K_v, v^*, w, \Delta t)$, where w denotes all the w_r-s for $r = 1, \ldots, N$ in (9). In case (iii), one needs to separate the real and imaginary parts and equate both of them to zero to obtain the stability boundary parameterized by θ.

While explicit solutions for parametric curves are difficult to obtain analytically, the boundaries can be found via a bisection method combined with continuation [50]. First, a trust region is created in the parameter space (e.g., in the (K_v, K_p)-plane) and a mesh grid is generated inside it. By checking the stability criterion at each grid point, we divide the trust region into stable and unstable regions that are separated by coarse boundaries. Then, bisection is used to refine the boundaries. Finally, interpolation-correction procedure can be applied repeatedly to further smooth the stability boundaries until the required accuracy and smoothness are achieved. The advantage of this method is that it works for a wide variety of problems, including non-smooth boundaries and non-convex stability domains.

Theorem 4 implies that stability of the second moment dynamics and the stability of the covariance dynamics are equivalent when the mean dynamics are stable. Consequently, only the plant stability for the second moment dynamics is discussed here. Similar to the mean dynamics, to ensure plant stability of the second moment dynamics $\hat{\bar{X}}(k+1) = \bar{\bar{\mathbf{A}}}\hat{\bar{X}}(k)$ [cf. (36) with $U(k) = 0$ and $\bar{\bar{\mathbf{A}}}$ as defined in (40)], all the eigenvalues $z \in \mathbb{C}$ of the matrix $\bar{\bar{\mathbf{A}}}$ must lie within the unit circle in the complex plane. These eigenvalues are given by the characteristic equation

$$\det(z\,\bar{\bar{\mathbf{I}}} - \bar{\bar{\mathbf{A}}}) = 0 \tag{42}$$

where $\bar{\bar{\mathbf{I}}} \in \mathbb{R}^{4(N+1)^2 \times 4(N+1)^2}$ is the identity matrix. The corresponding stability boundaries can be obtained as explained above for the three different kinds of stability losses.

Fig. 4(a) shows the plant stability diagram in the (K_v, K_p)-plane for the parameters $v_{\max} = 30$ [m/s], $h_{\text{st}} = 5$ [m], $h_{\text{go}} = 35$ [m], $v^* = 15$ [m/s] [cf. (12), (14)], which will be kept the same throughout the whole paper. Here, we also consider the packet delivery ratio $p = 0.8$ and the sampling time $\Delta t = 0.1$ [s]. For the mean dynamics (31), the horizontal red line and the red curve correspond to the critical cases (i) and (iii), respectively. The oscillation frequency is zero along the horizontal red line while the frequency $\theta/\Delta t$ increases monotonously along the red curve, that is, the further we are from the origin (along the curve), the higher the frequency of the arising oscillations is. The region enclosed by these curves, i.e., the union of the red and purple shaded regions, is the mean plant stable region. For the second moment dynamics (36), the purple horizontal line and purple curve both correspond to the critical case (i). The purple shaded region enclosed by these two curves is the second moment plant stable region. In this case the oscillation frequency is zero along the horizontal purple line as well as

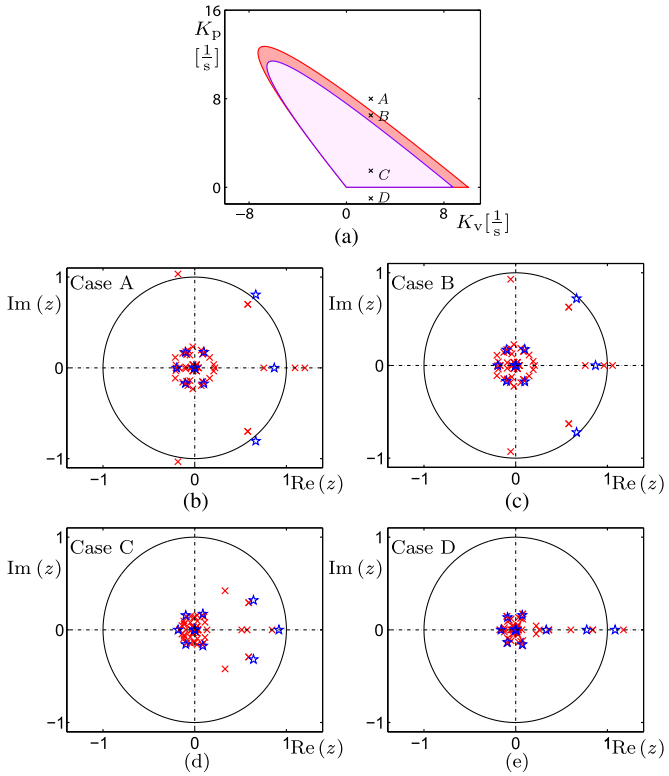

Fig. 4. (a) Plant stability diagrams in the (K_v, K_p)-plane for $p = 0.8$, $\Delta t = 0.1$ [s], and IID assumption. Red and purple curves correspond to changes in plant stability of the mean dynamics and the second moment dynamics, respectively. Red and purple shaded regions correspond to plant stable domains of the mean dynamics and second moment dynamics, respectively. (b)–(e) Blue stars and red crosses mark the root loci of the mean dynamics and the second moment dynamics on the z-domain, respectively, corresponding to the points A–D marked on (a).

along the purple curve, implying that the covariance can only lose plant stability via non-oscillatory divergence.

The root loci for the points A-D marked in Fig. 4(a) are plotted in Fig. 4(b)–(e). Blue stars indicate the roots of (41) for the mean while red crosses indicate the roots of (42) for the second moment. In case A, there are two eigenvalues located outside the unit circle for the mean dynamics and four for the second moment dynamics. As K_p decreases, the eigenvalues of the mean dynamics move inside the unit circle while there is still one eigenvalue outside the unit circle for the second moment dynamics, as shown in case B. Decreasing K_p further, the eigenvalues of the second moment dynamics also move inside the unit circle as shown in case C and the system becomes stable. Decreasing K_p even further, a pair of complex conjugate eigenvalues "meet" at the real axis for the mean dynamics and then they split into two real eigenvalues. One of them crosses the unit circle at 1 and moves outside as shown in Case D. Meanwhile, an eigenvalue for the second moment dynamics also moves outside the unit circle at 1.

B. String Stability

String stability is achieved when the follower is capable of attenuating the fluctuations of the leader's velocity. For deterministic linear systems string stability is equivalent to the attenuation of sinusoidal signals at all frequencies, which can be evaluated using transfer functions [27], [51]. However, an equivalent notion of string stability does not exist for stochastic systems. One may use the mean dynamics (31) to characterize string stability as this provides a necessary condition for the string stability of the stochastic system (25). However, this may still allow a large fraction of trajectories to be string unstable. To resolve this issues we use the covariance dynamics (39) to establish the concept of $n\sigma$ string stability. This guarantees that all trajectories within a neighborhood of radius n times the standard deviation about the mean are string stable (i.e., the amplification ratio is less than 1 for trajectories within this set). This characterization allows us to design controllers that are robust against stochastic delay variations to a given degree.

We consider the periodic input $\tilde{v}_L(t)$ given in (16) and the output $\tilde{v}(t)$. After discretizing time [cf. (17), (19)], we obtain two discrete inputs $\tilde{v}_L(k)$ and $\tilde{v}_L^{\perp}(k)$, and one discrete output $\tilde{v}(k)$. However, the inputs are not linearly independent, so their effect has to be summed up.

To evaluate the string stability of the mean dynamics, we apply Z transform to (31), to obtain the transfer function between the input $U(k)$ and the output $\bar{Y}(k)$ as

$$\begin{bmatrix}\bar{\gamma}_1(z) & \bar{\gamma}_2(z)\end{bmatrix} := \bar{\mathbf{C}}(z\,\bar{\mathbf{I}} - \bar{\mathbf{A}})^{-1}\bar{\mathbf{B}}. \tag{43}$$

To simplify the notations, $\bar{\gamma}_1$ and $\bar{\gamma}_2$ will be used in lieu of $\bar{\gamma}_1(\mathrm{e}^{\mathrm{j}\omega\Delta t})$ and $\bar{\gamma}_2(\mathrm{e}^{\mathrm{j}\omega\Delta t})$, respectively. In linear time invariant systems, the steady state output of $\bar{Y}(k)$ can be expressed as the summation of the contribution of each individual input. By applying trigonometric identities and Euler's formula, the steady state output can be written as

$$\begin{aligned}\bar{Y}_{\mathrm{ss}}(k) &= |\bar{\gamma}_1|\tilde{v}_L^{\mathrm{amp}}\sin(k\omega\Delta t + \angle\bar{\gamma}_1)\\ &\quad + |\bar{\gamma}_2|\tilde{v}_L^{\mathrm{amp}}\cos(k\omega\Delta t + \angle\bar{\gamma}_2)\\ &= \bar{M}(\omega)\tilde{v}_L^{\mathrm{amp}}\sin\left(k\omega\Delta t + \bar{\psi}(\omega)\right)\end{aligned} \tag{44}$$

where the amplification ratio and phase lag are given by

$$\begin{aligned}\bar{M}(\omega) &= \sqrt{|\bar{\gamma}_1|^2 + |\bar{\gamma}_2|^2 + 2\,\mathrm{Im}(\bar{\gamma}_1\bar{\gamma}_2^*)} = |\bar{\gamma}_1 + \mathrm{j}\bar{\gamma}_2|\\ \bar{\psi}(\omega) &= \arctan\frac{\mathrm{Im}(\bar{\gamma}_1) + \mathrm{Re}(\bar{\gamma}_2)}{\mathrm{Re}(\bar{\gamma}_1) - \mathrm{Im}(\bar{\gamma}_2)} = \angle\left(\bar{\gamma}_1 + \mathrm{j}\bar{\gamma}_2\right)\end{aligned} \tag{45}$$

respectively, and $*$ denotes the complex conjugate. Thus

$$\bar{M}(\omega) = \left|\bar{\Gamma}(e^{\mathrm{j}\omega\Delta t})\right|, \quad \bar{\psi}(\omega) = \angle\bar{\Gamma}(e^{\mathrm{j}\omega\Delta t}) \tag{46}$$

where

$$\bar{\Gamma}(z) = \begin{bmatrix}\bar{\gamma}_1(z) & \bar{\gamma}_2(z)\end{bmatrix}\bar{\mathbf{E}} = \bar{\mathbf{C}}\left(z\,\bar{\mathbf{I}} - \bar{\mathbf{A}}\right)^{-1}\bar{\mathbf{B}}\bar{\mathbf{E}} \tag{47}$$

$$\bar{\mathbf{E}} = \begin{bmatrix}1 & \mathrm{j}\end{bmatrix}^{\mathsf{T}}. \tag{48}$$

The condition for mean string stability is given by

$$\sup_{\omega>0}\ \bar{M}(\omega) < 1 \tag{49}$$

yielding the string stability boundaries

$$\begin{cases} \bar{M}(\bar{\omega}_{\text{cr}}) = 1 \\ \bar{M}'(\bar{\omega}_{\text{cr}}) = 0 \end{cases} \tag{50}$$

for the critical excitation frequency $\bar{\omega}_{\text{cr}} > 0$, where prime denotes differentiation with respect to ω. Note that $\bar{M}$ also depends on the parameters $(K_p, K_v, w, v^*, \Delta t)$. Similarly to the plant stability boundaries, the parametric string stability boundary (50) cannot be obtained analytically but can be found using the bisection method. Finally, one may show that $\bar{M}(0) = 1$, $\bar{M}'(0) = 0$ always hold. Therefore, string stability requires $\bar{M}''(0) < 0$ and the corresponding boundary is given by

$$\bar{M}''(0) = 0. \tag{51}$$

Equation (39) describing covariance dynamics is nonlinear and also contains terms driven by the mean dynamics (31). For determining $n\sigma$ string stability only the steady state dynamics of the mean and the covariance are needed, but the covariance dynamics (39) do not provide a direct input-output relationship like the mean dynamics (31) do. To simplify the analysis, we assume that the mean dynamics are plant stable and already at steady state. In this case, the steady state response shares the same form with the input, i.e., it is a sinusoidal signal. Thus, at steady state, one can assume

$$\bar{X}(k) = \mathbf{Q}U(k). \tag{52}$$

Substituting this into the mean dynamics (31) and using the property (22), one can get

$$\mathbf{Q} - \bar{\mathbf{A}}\mathbf{Q}\mathbf{R} = \bar{\mathbf{B}}\mathbf{R} \tag{53}$$

which can be rewritten into the form

$$(\mathbf{I} \otimes \bar{\mathbf{I}} - \mathbf{R}^{\mathrm{T}} \otimes \bar{\mathbf{A}})\overline{\text{vec}}(\mathbf{Q}) = \overline{\text{vec}}(\bar{\mathbf{B}}\mathbf{R}) \tag{54}$$

with the help of property (2). We remark that $\mathbf{Q}$ can also be obtained by using transfer functions, cf. (43), (44). Substituting equation (52) into (39) yields the simplified covariance dynamics

$$\begin{aligned} \bar{\bar{X}}(k+1) &= \bar{\bar{\mathbf{A}}}\bar{\bar{X}}(k) + \bar{\bar{\mathbf{B}}}\bar{\bar{U}}(k) \\ \bar{\bar{Y}}(k) &= \bar{\bar{\mathbf{C}}}\bar{\bar{X}}(k) \end{aligned} \tag{55}$$

where

$$\bar{\bar{U}}(k) = U(k) \otimes U(k) \tag{56}$$

and $\bar{\bar{\mathbf{A}}}$ and $\bar{\bar{\mathbf{C}}}$ are given by (40), while

$$\begin{aligned} \bar{\bar{\mathbf{B}}} &= \bar{\bar{\mathbf{H}}}_1(\mathbf{Q} \otimes \mathbf{I}) + \bar{\bar{\mathbf{H}}}_2(\mathbf{I} \otimes \mathbf{Q}) + \bar{\bar{\mathbf{H}}}_3(\mathbf{I} \otimes \mathbf{I}) + \bar{\bar{\mathbf{H}}}_4(\mathbf{Q} \otimes \mathbf{Q}) \\ &= \sum_{r=1}^{N} w_r(\mathbf{A}_r\mathbf{Q} + \mathbf{B}_r) \otimes (\mathbf{A}_r\mathbf{Q} + \mathbf{B}_r) \\ &\quad - (\bar{\mathbf{A}}\mathbf{Q} + \bar{\mathbf{B}}) \otimes (\bar{\mathbf{A}}\mathbf{Q} + \bar{\mathbf{B}}). \end{aligned} \tag{57}$$

By substituting the input (17) into (56), one may notice that the input $\bar{\bar{U}}(k)$ can be separated into a constant part and a harmonic excitation part, i.e.,

$$\bar{\bar{U}}(k) = \bar{\bar{U}}_0 + \bar{\bar{U}}_1(k) \tag{58}$$

where

$$\bar{\bar{U}}_0 = \frac{1}{2}\left(v_L^{\text{amp}}\right)^2 \bar{\bar{u}}_0,\ \bar{\bar{U}}_1(k) = \frac{1}{2}\left(v_L^{\text{amp}}\right)^2 \bar{\bar{u}}_1(k) \tag{59}$$

$$\bar{\bar{u}}_0 = \begin{bmatrix} 1 \\ 0 \\ 0 \\ 1 \end{bmatrix}, \quad \bar{\bar{u}}_1(k) = \begin{bmatrix} -\cos(2k\omega\Delta t) \\ \sin(2k\omega\Delta t) \\ \sin(2k\omega\Delta t) \\ \cos(2k\omega\Delta t) \end{bmatrix}. \tag{60}$$

According to superposition principle, the particular solution of the linear system (55) is the sum of particular solution $\bar{\bar{Y}}_0$ to $\bar{\bar{U}}_0$ and particular solution $\bar{\bar{Y}}_1(k)$ to $\bar{\bar{U}}_1(k)$. For input $\bar{\bar{U}}_0$, the response of the system (55) is given by

$$\bar{\bar{Y}}_0 = \left(v_L^{\text{amp}}\right)^2 \bar{\bar{M}}_0(\omega) \tag{61}$$

with

$$\bar{\bar{M}}_0(\omega) = \frac{1}{2}\bar{\bar{\mathbf{C}}}\left(\bar{\bar{\mathbf{I}}} - \bar{\bar{\mathbf{A}}}\right)^{-1}\bar{\bar{\mathbf{B}}}\bar{\bar{u}}_0. \tag{62}$$

For $\bar{\bar{U}}_1(k)$, similar to mean dynamics, taking the Z-transform of (55) and summing the contributions of each individual inputs of $\bar{\bar{u}}_1(k)$ in (60). Thus, we obtain the corresponding steady state output

$$\bar{\bar{Y}}_{1,\text{ss}}(k) = \left(v_L^{\text{amp}}\right)^2 \bar{\bar{M}}_1(\omega)\sin\left(2k\omega\Delta t + \bar{\bar{\psi}}(\omega)\right). \tag{63}$$

with

$$\bar{\bar{M}}_1(\omega) = \left|\bar{\bar{\Gamma}}(e^{\mathrm{j}\omega\Delta t})\right|, \quad \bar{\bar{\psi}}(\omega) = \angle\bar{\bar{\Gamma}}(e^{\mathrm{j}\omega\Delta t}) \tag{64}$$

where

$$\bar{\bar{\Gamma}}(z) = \frac{1}{2}\bar{\bar{\mathbf{C}}}\left(z\,\bar{\bar{\mathbf{I}}} - \bar{\bar{\mathbf{A}}}\right)^{-1}\bar{\bar{\mathbf{B}}}\bar{\bar{\mathbf{E}}} \tag{65}$$

$$\bar{\bar{\mathbf{E}}} = \begin{bmatrix} -\mathrm{j} & 1 & 1 & \mathrm{j} \end{bmatrix}^T. \tag{66}$$

Therefore, the superposition principle yields that the steady state response to (58) is

$$\begin{aligned} \bar{\bar{Y}}_{\text{ss}}(k) &= \bar{\bar{Y}}_0 + \bar{\bar{Y}}_{1,\text{ss}}(k) \\ &= \left(v_L^{\text{amp}}\right)^2 \left(\bar{\bar{M}}_0(\omega) + \bar{\bar{M}}_1(\omega)\sin\left(2k\omega\Delta t + \bar{\bar{\psi}}(\omega)\right)\right). \end{aligned} \tag{67}$$

Recall that $\bar{Y}(k) = \mathbb{E}[\tilde{v}(k)] \in \mathbb{R}$ and $\bar{\bar{Y}}(k) = \mathbb{E}[\tilde{v}^2(k)] - \mathbb{E}[\tilde{v}(k)]^2 \in \mathbb{R}$ and define

$$\mu = \bar{Y}_{\text{ss}}(k), \quad \sigma^2 = \bar{\bar{Y}}_{\text{ss}}(k) \tag{68}$$

respectively, as the mean and variance of $\tilde{v}(k)$ at steady state. Note that the variance $\bar{\bar{Y}}(k)$ is non-negative, and thus, (67) implies $\bar{\bar{M}}_0(\omega) \geq \bar{\bar{M}}_1(\omega)$.

From Chebyshev's inequality [52], we know that the probability of $\tilde{v}(k)$ being outside the window $[\mu - n\sigma, \mu + n\sigma]$, $n \in \mathbb{R}^+$ is rather small when $n \geq 1$. Therefore, using (44) and (67), we calculate

$$\mu \pm n\sigma = v_L^{\text{amp}} \left[\bar{M}(\omega) \sin\left(k\omega\Delta t + \bar{\psi}(\omega)\right) \pm n \sqrt{\bar{\bar{M}}_0(\omega) + \bar{\bar{M}}_1(\omega) \sin\left(2k\omega\Delta t + \bar{\bar{\psi}}(\omega)\right)} \right] \tag{69}$$

which is a periodic function with period $T = 2\,\pi/(\omega\Delta t)$. Thus, the total amplification ratio becomes

$$\bar{\bar{M}}(\omega) = \max_{0 \leq k \leq T} \left\{ \left| \bar{M}(\omega) \sin\left(k\omega\Delta t + \bar{\psi}(\omega)\right) \pm n \sqrt{\bar{\bar{M}}_0(\omega) + \bar{\bar{M}}_1(\omega) \sin\left(2k\omega\Delta t + \bar{\bar{\psi}}(\omega)\right)} \right| \right\}. \tag{70}$$

Definition 5: The system is said to be $n\sigma$ *string stable* if the amplitude of the input $\tilde{v}_L(k)$ is attenuated such that $|\mu \pm n\sigma| < v_L^{\text{amp}}$, i.e., the oscillations are constrained in the interval $[\mu - n\sigma, \mu + n\sigma]$.

Henceforth, the condition for $n\sigma$ string stability is given by

$$\sup_{\omega > 0} \bar{\bar{M}}(\omega) < 1 \tag{71}$$

and the corresponding boundaries can be found by bisection. Note that when $n = 0$, the $n\sigma$ string stability gives the mean string stability.

Fig. 5(a) shows the $n\sigma$ string stability diagram in the (K_v, K_p)-plane for packet delivery ratio $p = 0.8$ and sampling time $\Delta t = 0.1$[s] for different values of n. The green curve and the green straight lines correspond to the mean string stability boundaries (50) and (51), respectively. The union of the green and blue shaded regions enclosed by these curves is the mean string stable region. The blue curves correspond to the $n\sigma$ string stability boundaries for $n = 1$, 2, 3, respectively. The blue shaded region corresponds to the 1σ string stable region. For the mean dynamics, the critical frequency $\bar{\omega}_{\text{cr}}$ is zero along the straight lines but positive along the curve, and similar behavior occurs for the covariance dynamics.

The amplification ratios for the mean and covariance dynamics are plotted in Fig. 5(b)–(e) for $n = 1$ corresponding to the points E–H marked in Fig. 5(a). In case E, the system is mean string unstable for $0 < \omega < \bar{\omega}$ and 1σ string unstable for $0 < \omega < \bar{\bar{\omega}}$, but string stable in both sense for larger frequencies. As K_v is increased, the amplification ratios (45), (70) go below 1 for all frequencies, leading to mean string stability and $n\sigma$ string stability as shown in case F. However, as K_v is increased further, another peak of the amplification ratio (70) arises, resulting in the system being 1σ string unstable in the frequency domain $\underline{\underline{\omega}} < \omega < \bar{\bar{\omega}}$ as shown in case G. As K_v is increased even further, a similar peak of the mean amplification ratio (45) appears, and the system becomes mean string unstable for $\underline{\omega} < \omega < \bar{\omega}$.

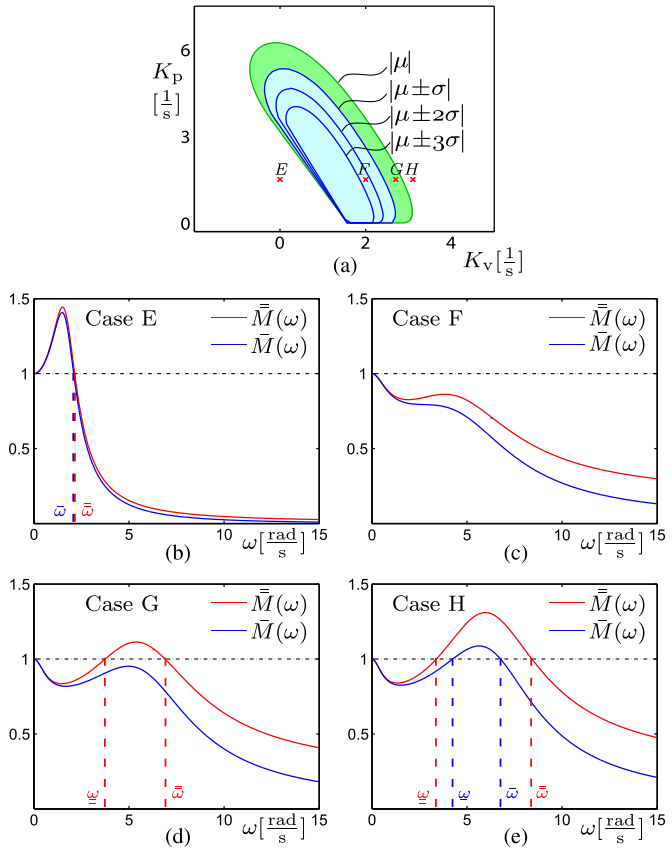

Fig. 5. (a) String stability diagrams in the (K_v, K_p)-plane for $p = 0.8$, $\Delta t = 0.1$ [s], and IID delay assumption. Green and blue curves correspond to changes in mean string stability and $n\sigma$ string stability, respectively. Green shaded and blue shaded regions correspond to mean string stable and 1σ string stable regions, respectively. (b)–(e) Blue and red curves represent the amplification ratios (45) and (70) for $n = 1$ as functions of the excitation frequency ω corresponding to the points E–H marked in (a).

C. Stability Charts

Fig. 6 shows the stability charts in the (K_v, K_p)-plane for different values of the packet delivery ratio p and sampling time Δt. The inlets show the probability distribution of the discrete stochastic delay given by (8). The same color scheme is used as in Figs. 4(a) and 5(a). The mean string stable domains and the 1σ string stable domains are embedded in the corresponding plant stable regions. We remark that there are some other string stable domains outside the plant stable domain which are not shown here. For plant stability, both the mean and covariance plant stable domains shrink as the packet delivery ratio p decreases and as sampling time Δt increases. Similar behavior can be observed for the mean string stable and 1σ string stable domains. When exceeding critical values, the string stable domains disappear, in which case there exist no gain combinations that can maintain string stability. Table I shows the approximate critical packet delivery ratio p_{cr} for different sampling time Δt.

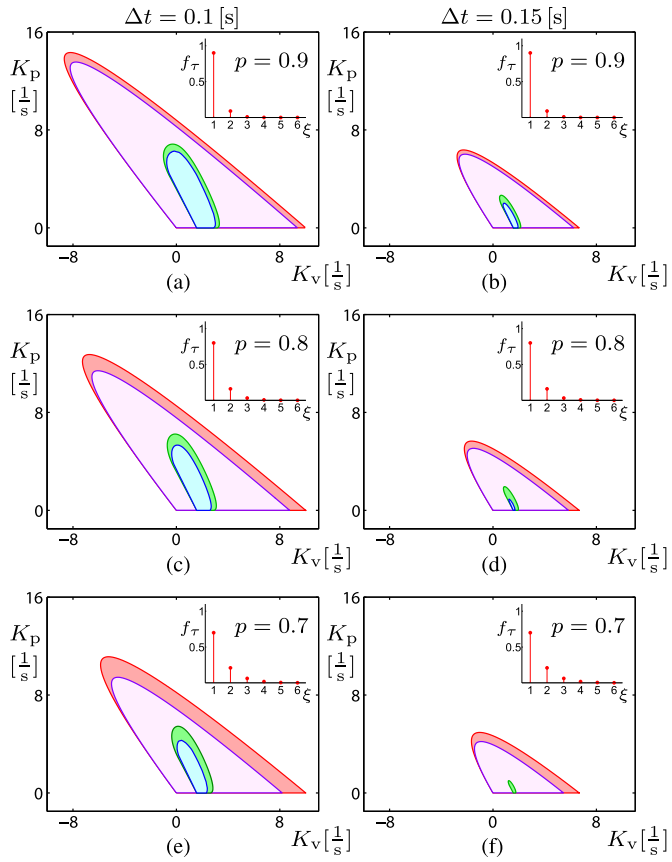

Fig. 6. Stability diagrams in the (K_v, K_p)-plane for different values of packet delivery ratio p and sampling time Δt as indicated and IID delay assumption. The corresponding delay distributions (8) are plotted on each panel as inlets. The same notation is used in Figs. 4(a) and 5(a).

TABLE I
CRITICAL SUCCESSFUL PACKET DELIVERY RATIO FOR DIFFERENT VALUES OF THE SAMPLING TIME

Δt [s]	0.1	0.15	0.2
$p_{\rm cr}$	0.35	0.62	0.92

V. REAL STOCHASTIC DELAY DYNAMICS

So far the stability condition for the stochastic system (25) have been derived while having the simplifying assumption of IID delay variations. However, as mentioned above, considering the stochastic delay dynamics (7), the system (25) describes a non-Markovian stochastic process, since $\mathbf{A}_{\tau(k)}$ and $\mathbf{B}_{\tau(k)}$ depends on $\mathbf{A}_{\tau(k-1)}$ and $\mathbf{B}_{\tau(k-1)}$. To handle this problem, here we select a subsequence from the dynamics (25) such that the new stochastic variable is IID and the resulting dynamics are described by a Markovian stochastic process. Then we apply the tools developed in Section IV to analyze the dynamics.

Let us consider the subsequence of states $X(k_l)$, inputs $U(k_l)$ and outputs $Y(k_l)$ at time instants k_l where $\tau(k_l) = 1$, cf. Fig. 7(a), that is, where new packets are delivered successfully, and denote them

$$\tilde{X}(l) = X(k_l), \quad \tilde{U}(l) = U(k_l), \quad \tilde{Y}(l) = Y(k_l). \tag{72}$$

Also, define $\tilde{\tau}(l) = \tau(k_l - 1)$, cf. Fig. 7(c), which is the maximum delay in the time interval $[k_{l-1}\Delta t,\ k_l\Delta t]$. This construction implies that $\tilde{\tau}(l)$-s are independently, identically distributed with the probability distribution function

$$f_{\tilde{\tau}(l)}(\xi) = \sum_{r=1}^{\infty} w_r \delta(\xi - r) \tag{73}$$

where w_r is given by (9). The counter k_l and the delay $\tilde{\tau}(l)$ are shown in Fig. 7(b) and (c), respectively.

Using system dynamics (25) recursively between k_l and k_{l+1} and exploiting the input property (22), we can obtain

$$\begin{aligned} \tilde{X}(l+1) &= \tilde{\mathbf{A}}_{\tilde{\tau}(l)}\, \tilde{X}(l) + \tilde{\mathbf{B}}_{\tilde{\tau}(l)}\, \tilde{U}(l) \\ \tilde{Y}(l) &= \mathbf{C}\, \tilde{X}(l) \end{aligned} \tag{74}$$

where $\tilde{\mathbf{A}}_{\tilde{\tau}(l)} \in \mathbb{R}^{2(N+1)\times 2(N+1)}$ and $\tilde{\mathbf{B}}_{\tilde{\tau}(l)} \in \mathbb{R}^{2(N+1)\times 2}$ can take values

$$\begin{aligned} \tilde{\mathbf{A}}_r &= \prod_{i=1}^{r} \mathbf{A}_i, \qquad r = 1,\ \ldots,\ N \\ \tilde{\mathbf{B}}_r &= \begin{cases} \mathbf{B}_1, & r = 1 \\ \mathbf{A}_r \tilde{\mathbf{B}}_{r-1} + \mathbf{B}_r (\mathbf{R}^{-1})^{r-1}, & r = 2,\ \ldots, N. \end{cases} \end{aligned} \tag{75}$$

Here, $\tilde{\mathbf{A}}_{\tilde{\tau}(l)}$ are independently, identically distributed, which is also the case for $\tilde{\mathbf{B}}_{\tilde{\tau}(l)}$, meaning that system (74) describes a discrete-time Markov process and stability in the second moment implies almost sure stability, cf. Theorem 5. Also, for $\tilde{\mathbf{A}}_{\tilde{\tau}(l)}$ and $\tilde{\mathbf{B}}_{\tilde{\tau}(l)}$, the joint PDF and the marginal PDF-s have the same form as (28) and (29), respectively. Finally, notice that $\tilde{\mathbf{A}}_{\tilde{\tau}(l)}$ and $\tilde{X}(l)$ are mutually independent, which is also the case for $\tilde{\mathbf{B}}_{\tilde{\tau}(l)}$ and $\tilde{X}(l)$. Now we can state that the stochastic system (25) subject to stochastic delays described by (7) is stable if and only if system (74) subject to (73) is stable in the same sense. This is because there are finitely many jumps between time instants l and $(l+1)$, since $(k_{l+1} - k_l) \leq N$ and because during each jump, the matrix $\mathbf{A}_r$ has a finite norm for any $r \in \{1, 2, \ldots, N\}$. Thus, the stability of the subsequence (at time instants k_l) ensures the stability of the whole sequence (at time instants k). Henceforth, the stability of the system (74) gives us the same stability as the original system.

Following the same method as in Section IV, one can obtain the mean dynamics:

$$\begin{aligned} \bar{X}(l+1) &= \bar{\mathbf{A}}\, \bar{X}(l) + \bar{\mathbf{B}}\, \tilde{U}(l) \\ \bar{Y}(l) &= \bar{\mathbf{C}}\, \bar{X}(l) \end{aligned} \tag{76}$$

by redefining the state and output as

$$\bar{X}(l) = \mathbb{E}\Big[\tilde{X}(l)\Big], \quad \bar{Y}(l) = \mathbb{E}\Big[\tilde{Y}(l)\Big] \tag{77}$$

and the matrices as

$$\bar{\mathbf{A}} = \sum_{r=1}^{N} w_r \tilde{\mathbf{A}}_r, \quad \bar{\mathbf{B}} = \sum_{r=1}^{N} w_r \tilde{\mathbf{B}}_r, \quad \bar{\mathbf{C}} = \mathbf{C} \tag{78}$$

cf. (30)–(32). Also, the covariance dynamics under the assumption that the mean is in steady state is given by

$$\begin{aligned} \bar{\bar{X}}(l+1) &= \bar{\bar{\mathbf{A}}} \bar{\bar{X}}(l) + \bar{\bar{\mathbf{B}}} \bar{\bar{U}}(l) \\ \bar{\bar{Y}}(l) &= \bar{\bar{\mathbf{C}}} \bar{\bar{X}}(l) \end{aligned} \tag{79}$$

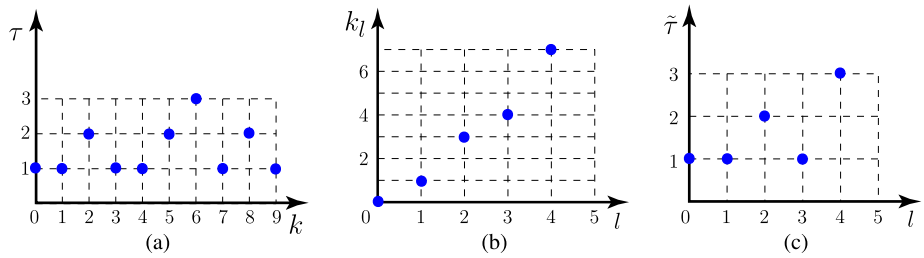

Fig. 7. (a) Stochastic delays in the discrete-time system (15). (b) Relationship between counters l and k_l. (c) Number of trials $\tilde{\tau}$ at time instant l until a new packet is received at $k_l\Delta t$.

where the states are defined as

$$\bar{\bar{X}}(l) = \mathbb{E}\left[\tilde{X}(l)\otimes\tilde{X}(l)\right] - \bar{X}(l)\otimes\bar{X}(l)$$
$$\bar{\bar{Y}}(l) = \mathbb{E}\left[\tilde{Y}(l)\otimes\tilde{Y}(l)\right] - \bar{Y}(l)\otimes\bar{Y}(l)$$
$$\bar{\bar{U}}(l) = \tilde{U}(l)\otimes\tilde{U}(l) \tag{80}$$

the matrices are given by

$$\bar{\bar{\mathbf{A}}} = \sum_{r=1}^{N} w_r \tilde{\mathbf{A}}_r \otimes \tilde{\mathbf{A}}_r$$
$$\bar{\bar{\mathbf{B}}} = \sum_{r=1}^{N} w_r (\tilde{\mathbf{A}}_r\tilde{\mathbf{Q}} + \tilde{\mathbf{B}}_r)\otimes(\tilde{\mathbf{A}}_r\tilde{\mathbf{Q}} + \tilde{\mathbf{B}}_r) - (\bar{\mathbf{A}}\tilde{\mathbf{Q}} + \bar{\mathbf{B}})\otimes(\bar{\mathbf{A}}\tilde{\mathbf{Q}} + \bar{\mathbf{B}})$$
$$\bar{\bar{\mathbf{C}}} = \mathbf{C}\otimes\mathbf{C} \tag{81}$$

and $\tilde{\mathbf{Q}}$ is the solution of

$$\tilde{\mathbf{Q}} - \bar{\mathbf{A}}\tilde{\mathbf{Q}}\mathbf{R} = \bar{\mathbf{B}}\mathbf{R} \tag{82}$$

cf. (38), (40), (53), (55)–(57).

Following the same method as in Section IV-A, one can obtain the mean and covariance plant stability boundaries based on the characteristic equations (41) and (42), where $\bar{\mathbf{A}}$ and $\bar{\bar{\mathbf{A}}}$ are given by (78) and (81), respectively. Fig. 8(a) shows the plant stability diagram in the (K_v, K_p)-plane for the mean and covariance dynamics. The same color scheme is used as in Fig. 4(a). The stability domains in Fig. 8(a) are similar to those in Fig. 4(a) except that the size difference between the mean and covariance plant stable domains is larger. The root loci for points marked A–D in Fig. 8(a) are plotted in Fig. 8(b)–(e). Note that the locations of these points are the same as in Fig. 4(a). Comparing the corresponding panels in Figs. 4 and 8, one may notice that there are more zero eigenvalues in the second case, which is caused by the singularities in $\bar{\mathbf{A}}$ and $\bar{\bar{\mathbf{A}}}$ given in (78) and (81) coming from the singularity of $\tilde{\mathbf{A}}_r$-s in (75).

Similarly, following the same method as in Section IV-B, the mean and covariance string stability boundaries can be obtained based on the amplification ratios (45), (70), where ($\bar{\mathbf{A}}$, $\bar{\mathbf{B}}$, $\bar{\mathbf{C}}$) and ($\bar{\bar{\mathbf{A}}}$, $\bar{\bar{\mathbf{B}}}$, $\bar{\bar{\mathbf{C}}}$) are given in (78) and (81). Fig. 9(a) shows the $n\sigma$ string stability diagram in the (K_v, K_p)-plane, using the same color scheme as in Fig. 5(a). One may notice that the mean string stable domain is larger in Fig. 9(a), but the domain shrinks much faster as the value of n increases. In particular,

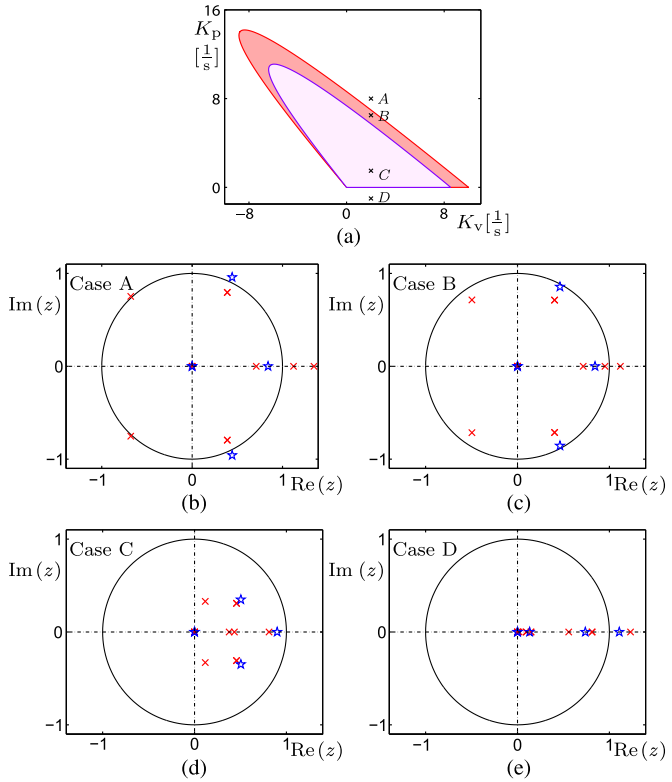

Fig. 8. (a) Plant stability diagrams in the (K_v, K_p)-plane for $p = 0.8$ and $\Delta t = 0.1$ [s], without IID delay assumption. The same color scheme is used in Fig. 4(a). (b)–(e) Blue stars and red crosses mark the root loci of the mean dynamics and the covariance dynamics on the z-domain, respectively, corresponding to the points A–D in (a).

the $n\sigma$ string stable domain disappears for $n = 3$ whereas it is still present in Fig. 5(a). This justifies that considering the correct stochastic delay dynamics is important. The amplification ratios for the mean and covariance dynamics are plotted in Fig. 9(b)–(e) corresponding to the points E–H marked in Fig. 9(a) that are at the same locations as those in Fig. 5(a). The curves look qualitatively similar to those in Fig. 5, except the height difference between the mean and the second moment amplification ratio curves.

Fig. 10 shows the stability charts in the (K_v, K_p)-plane for different values of the packet delivery ratio p and sampling time Δt. The same notations are used as in Fig. 6. The mean string stable domains and the 1σ string stable domain are embedded in the corresponding plant stable regions. In general, they look similar to those in Fig. 6, but one may also notice some

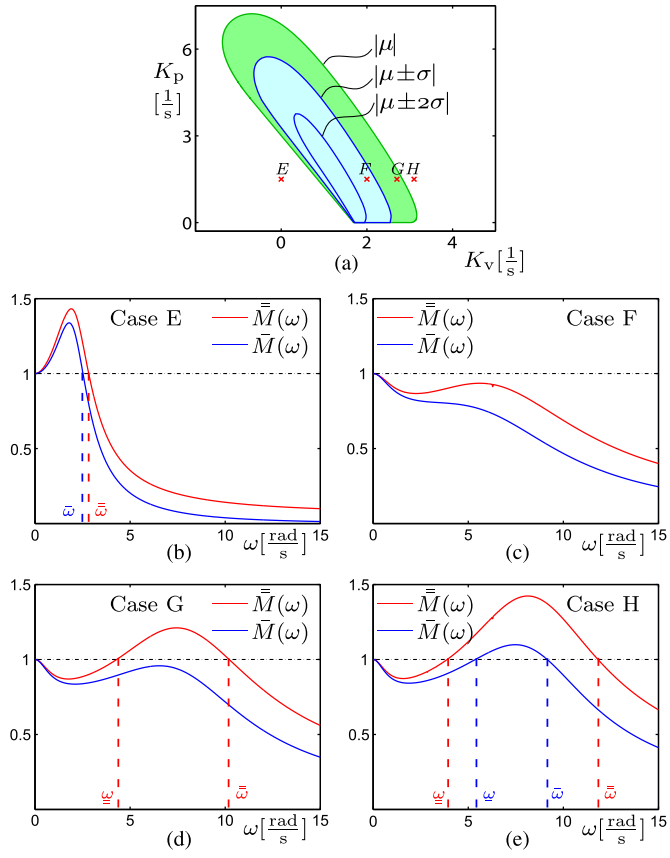

Fig. 9. (a) String stability diagrams in the (K_v, K_p)-plane for $p = 0.8$ and $\Delta t = 0.1$ [s], without IID delay assumption. The same color scheme is used in Fig. 5(a). (b)–(e) Blue and red curves represent the amplification ratios (45) and (70) for $n = 1$, respectively, as functions of the excitation frequency ω corresponding to the points E–H in (a).

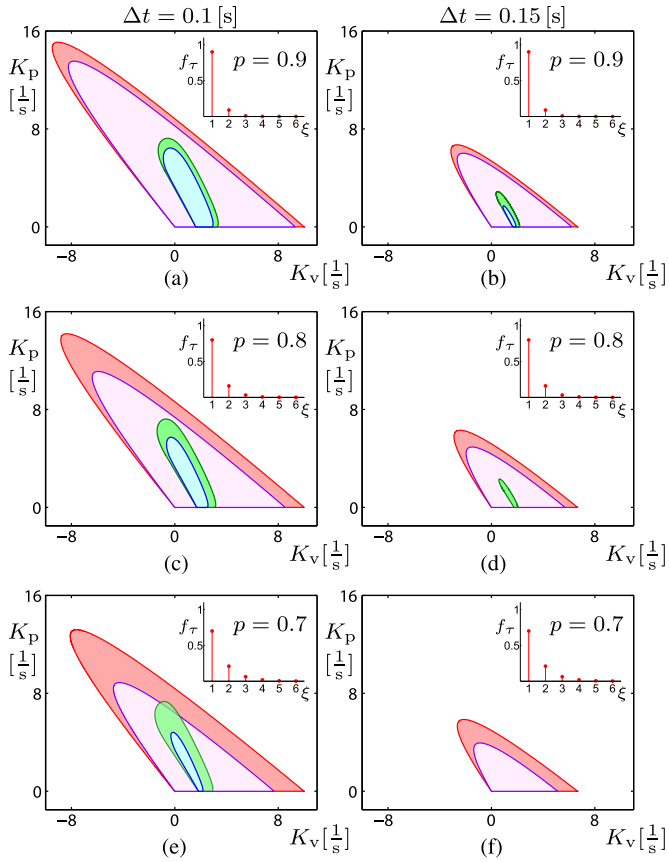

Fig. 10. Stability diagrams in the (K_v, K_p)-plane for different values of packet delivery ratio p and sampling time Δt as indicated and without IID delay assumption. The same notation is used as in Fig. 6.

differences. On one hand, the differences between mean plant stable domains and the covariance plant stable domains become larger compared to Fig. 6, and this also holds for the differences between the mean string stable domains and 1σ string stable domains. Moreover, the covariance stability domains shrink faster in Fig. 10 than in Fig. 6. Finally, there is an intersection between covariance plant stable domain and mean string stable domain in panel (e). These differences again justify that considering the correct stochastic delay dynamics is important.

In Section III, the geometric distribution was truncated with the maximum delay N based on a critical cumulative packet delivery ratio. To validate this truncation, stability diagrams for different N-s in the same parameter space can be compared to check whether the results converge to a certain limit as N increases. Our results show that for realistic values of the packet delivery ratio, the stability domains converge so fast that there is almost no difference between plant stability boundaries for $N = 3$ and $N \geq 4$, and between string stability boundaries for $N = 6$ and $N \geq 7$. This justifies our truncation method and validates our stability analysis for large N.

VI. Simulations

In this section, we use numerical simulation to demonstrate the stability results generated above for the real stochastic delay dynamics discussed in Section V. We show that the conditions of linear plant and string stability obtained above can give a guidance when selecting control gains to achieve desired behavior.

Fig. 11 shows the mean and 1σ window of 1000 numerical simulations for the linear stochastic system (19) on the left and for the nonlinear stochastic system (15) on the right, subject to the inputs $v_L(t) \equiv v_L^*$ and $\tilde{v}_L(t) \equiv 0$, cf. (16). Cases A–D correspond to the cases in Fig. 8. In case A, there are eigenvalues located outside the unit circle for the mean and covariance dynamics, and simulation results show that both the mean and variance of the velocity diverge in an oscillatory way. As K_p decreases, the mean dynamics become stable while the variance still diverges as shown in case B. Decreasing K_p more, the covariance dynamics are also stabilized as shown in case C, and both the mean and the variance converge to the equilibrium. Decreasing K_p even further, both the mean and the variance lose stability in a non-oscillatory way corresponding to the positive real roots outside the unit circle.

The linear system and nonlinear system show similar behavior in terms of plant stability, implying that the linear system can predict the stability of the nonlinear system in the neighborhood of the equilibrium. However, the linear system diverges faster than the nonlinear system, since the nonlinear system has some saturations that prevent the system from diverging to infinity. Most importantly, in case C, one can observe that

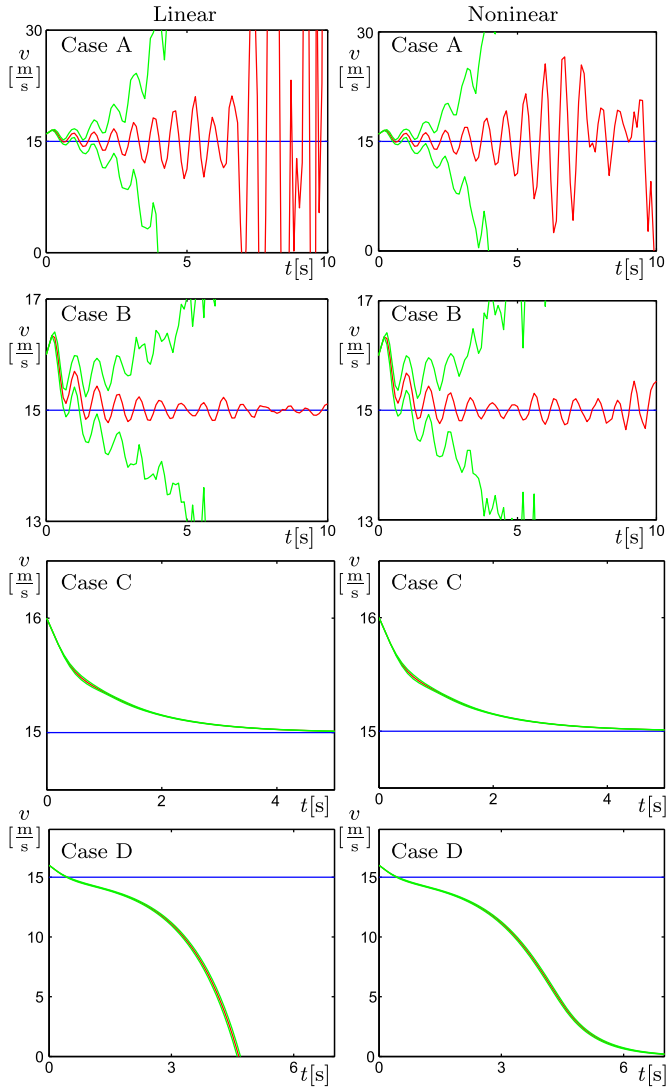

Fig. 11. Mean and 1σ window of 1000 simulations for the linear system (19) and nonlinear system (15) subject to constant inputs $v_L(t) \equiv v_L^*$ and $\tilde{v}_L(t) \equiv 0$ with the gains corresponding to the points marked A–D in Fig. 8(a). The initial perturbations are $\tilde{h}(t) = 10.2$ [m], $\tilde{v}(t) = 0.2$ [m/s], for $t \in [-\Delta t,\ 0]$. Blue curves represent the leader's velocity, red curves represent the follower's mean velocity, and green curves represent the follower's 1σ window.

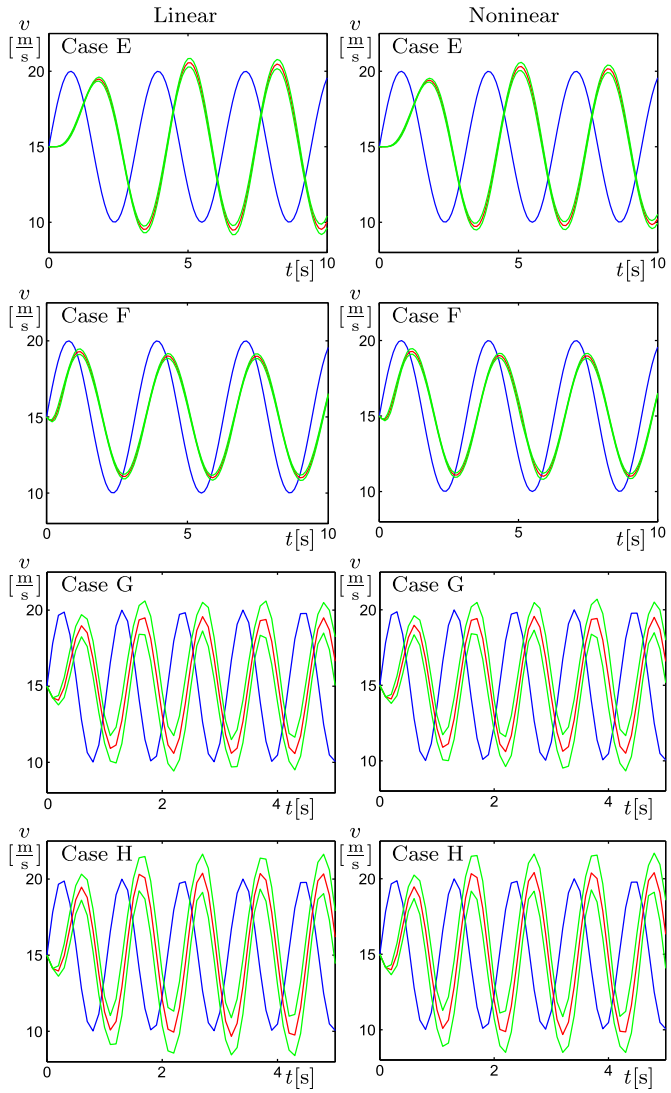

Fig. 12. Mean and 1σ window of 1000 simulations of the linear system (19) and the nonlinear system (15) subject to sinusoidal input (16) with $v_L^{\text{amp}} = 5$ [m/s] and the gains corresponding to the points E–H in Fig. 9(a). Here, $\omega = 2$ [rad/s] for the first two rows, and $\omega = 6$ [rad/s] for the last two rows. The initial conditions are chosen as $\tilde{h}(t) = 0$ [m] and $\tilde{v}(t) = 0$ [m/s], for $t \in [-\Delta t,\ 0]$. Blue curves represent the leader's velocity, red curves represent the follower's mean velocity, and green curves represent the follower's 1σ window.

the mean of the follower's velocity converges to the leader's velocity while the 1σ window converges to the mean, yielding that the variance converges to zero. Thus, the system in case C is almost surely stable even though it is subject to stochastic delay variations, which is our ultimate goal when designing a controller for a stochastic system.

Fig. 12 shows the mean and 1σ window of 1000 numerical simulations for the linear stochastic system (19) on the left and for the nonlinear stochastic system (15) on the right, subject to sinusoidal input (16) with $v_L^{\text{amp}} = 5$ [m/s]. Cases E–H correspond to the cases in Fig. 9. In case E, the system is mean string unstable and 1σ string unstable for lower frequencies. The corresponding simulations show that amplification indeed happens for excitation frequency $\omega = 2$ [rad/s]. As K_v is increased, the system becomes both mean string stable and 1σ string stable as shown in case F, and the amplitude of the sinusoidal input is attenuated for the mean as well as for the 1σ window. However, as K_v is increased further, the system becomes 1σ string unstable for higher frequencies as shown in case G. The corresponding simulations show amplification in the 1σ window but attenuation in the mean for the sinusoidal input with excitation frequency $\omega = 6$ [rad/s]. As K_v is increased even further, the system becomes string unstable both in terms of mean and covariance dynamics at higher frequencies and the corresponding simulations show amplification both in the mean and in the 1σ window as depicted in case H.

One may notice that there is not too much difference between the simulations of linear stochastic system and nonlinear stochastic systems, which again validates the use of the linearized system to test string stability. For larger variations, some discrepancies appear between them due to the saturation in the

nonlinear stochastic system. Furthermore, corresponding to the stochastic nature of packet drops, simulations show amplitude variations which are "not uniformly" string unstable. We emphasize that in case F we achieve our design goal since we achieve string stability for a system subject to stochastic delay variations. Finally, we remark that in some cases simulations show string stable behavior where analytical results predict high frequency ($\omega \geq 6$ [rad/s]) string instability. This is because high frequency signals are filtered by the low sampling rates ($\Delta t \geq 0.1$ [s]). Investigating such effects is left for future research.

VII. Conclusion

In this paper, the effects of stochastic delays on the dynamics of connected vehicles were studied by analyzing both the mean and covariance dynamics. Plant stability and $n\sigma$ string stability conditions were derived and it was shown that almost sure plant stability and $n\sigma$ string stability could be achieved up to a certain level of stochastic delay variations. We also demonstrated that the stability domains shrink when the packet drop ratio or the sampling time increases and above a critical limit string stability cannot be achieved by any gain combinations. This gives requirements for the sampling frequency and reliability of DSRC devices.

In the future we will pursue multiple research directions based on the results obtained in this paper. First of all, to fully exploit the advantages of CCC we will include information from vehicles beyond the line of sight [51] and will include information that is not attainable by range sensors (like acceleration) [22]. Moreover, we will consider higher fidelity vehicle models [23] and more sophisticated controllers [53]. Moreover, we will examine the Safety Pilot data [44] in order to extract the packet drop dynamics in real DSRC networks. Finally, we are planning to build a scaled experimental test bed that allows us to realize the controllers in practice.

Appendix

A Derivation of Equation (15)

By noticing that in the time interval $t \in [t_k,\ \ t_{k+1})$, $u(t_{k-\tau(k)})$ is a constant, one can solve the differential equation (10) directly with initial values $h(t_k), v(t_k)$ given at time instant t_k, which results in

$$\begin{aligned} h(t) &= h(t_k) + \int_{t_k}^{t_{k+1}} v_L(t)\,\mathrm{d}t - v(t_k)(t-t_k) \\ &\quad - \frac{1}{2}u(t_{k-\tau(k)})(t-t_k)^2 \\ v(t) &= v(t_k) + u(t_{k-\tau(k)})(t-t_k). \end{aligned} \tag{83}$$

Then by calculating the values at time instant $t = t_{k+1}$ and substituting $u(t_{k-\tau(k)})$ using (11), one can get the nonlinear map (15).

Acknowledgment

We thank Richard Murray and Mehdi Sadeghpour for the helpful discussions.

References

[1] D. Schrank, B. Eisele, and T. Lomax, "TTI's 2012 urban mobility report powered by INRIX traffic data," Texas A&M Transp. Inst., College Station, TX, USA, Tech. Rep., 2012.
[2] "2013 Motor vehicle crashes: Overview," USDOT, Nat. Highway Traffic Safety Admin., Washington, DC, USA, Tech. Rep., 2014.
[3] G. Orosz, R. E. Wilson, R. Szalai, and G. Stépán, "Exciting traffic jams: Nonlinear phenomena behind traffic jam formation on highways," *Phys. Rev. E*, vol. 80, no. 4, Oct. 2009, Art. no. 046205.
[4] D. Swaroop and J. K. Hedrick, "String stability of interconnected systems," *IEEE Trans. Autom. Control*, vol. 41, no. 3, pp. 349–357, Mar. 1996.
[5] S. E. Shladover, "Longitudinal control of automotive vehicles in close-formation platoons," *J. Dyn. Syst. Meas. Control*, vol. 113, no. 2, pp. 231–241, Jun. 1991.
[6] P. A. Ioannou and C. C. Chien, "Autonomous intelligent cruise control," *IEEE Trans. Veh. Technol.*, vol. 42, no. 4, pp. 657–672, Nov. 1993.
[7] R. Rajamani and C. Zhu, "Semi-autonomous adaptive cruise control systems," *IEEE Trans. Veh. Technol.*, vol. 51, no. 5, pp. 1186–1192, Sep. 2002.
[8] J. V. Werf, S. E. Shladover, M. A. Miller, and N. Kourjanskaia, "Effects of adaptive cruise control systems on highway traffic flow capacity," *Transp. Res. Rec., J. Transp. Res. Board*, vol. 1800, no. 1, pp. 78–84, 2002.
[9] L. C. Davis, "Effect of adaptive cruise control systems on traffic flow," *Phys. Rev. E*, vol. 69, no. 6, Jun. 2004, Art. no. 066110.
[10] *Part 11: Wireless LAN Medium Access Control (MAC) and Physical Layer (PHY) Specifications, Amendment 6: Wireless Access in Vehicular Environments*, IEEE Std. 802.11p-2010, 2010, pp. 1–51.
[11] J. B. Kenney, "Dedicated Short-Range Communications (DSRC) standards in the United States," *Proc. IEEE*, vol. 99, no. 7, pp. 1162–1182, Jul. 2011.
[12] G. J. L. Naus, R. P. A. Vugts, J. Ploeg, M. R. J. G. van de Molengraft, and M. Steinbuch, "String-stable CACC design and experimental validation: A frequency-domain approach," *IEEE Trans. Veh. Technol.*, vol. 59, no. 9, pp. 429–436, Nov. 2010.
[13] C. Desjardins and B. Chaib-draa, "Cooperative adaptive cruise control: A reinforcement learning approach," *IEEE Trans. Intell. Transp. Syst.*, vol. 12, no. 4, pp. 1248–1260, Dec. 2011.
[14] V. Milanes, S. E. Shladover, J. Spring, C. Nowakowski, H. Kawazoe, and M. Nakamura, "Cooperative adaptive cruise control in real traffic situations," *IEEE Trans. Intell. Transp. Syst.*, vol. 15, no. 1, pp. 296–305, Feb. 2014.
[15] J. Ploeg, D. P. Shukla, N. van de Wouw, and H. Nijmeijer, "Controller synthesis for string stability of vehicle platoons," *IEEE Trans. Intell. Transp. Syst.*, vol. 15, no. 2, pp. 854–865, Apr. 2014.
[16] Y. Zheng, S. E. Li, J. Wang, D. Cao, and K. Li, "Stability and scalability of homogeneous vehicular platoon: Study on the influence of information flow topologies," *IEEE Trans. Intell. Transp. Syst.*, vol. 17, no. 1, pp. 14–26, Jan. 2016.
[17] R. Rajamani and S. E. Shladover, "An experimental comparative study of autonomous and co-operative vehicle-follower control systems," *Transp. Res. C, Emerging Technol.*, vol. 9, no. 1, pp. 15–31, Feb. 2001.
[18] E. Chan, P. Gilhead, P. Jelínek, P. Krejčí, and T. Robinlerative control of SARTRE automated platoon vehicles," in *Proc. 19th ITS World Congr.*, Vienna, Austria, 2012, pp. 1–9.
[19] J. Ploeg, S. Shladover, H. Nijmeier, and N. V. de Wouw, "Introduction to the special issue on the 2011 grand cooperative driving challenge," *IEEE Trans. Intell. Transp. Syst.*, vol. 13, no. 3, pp. 989–993, Sep. 2012.
[20] E. van Nunen, M. R. J. A. E. Kwakkernaat, J. Ploeg, and B. D. Netten, "Cooperative competition for future mobility," *IEEE Trans. Intell. Transp. Syst.*, vol. 13, no. 3, pp. 1018–1025, Sep. 2012.
[21] B. van Arem, C. J. G. van Driel, and R. Visser, "The impact of cooperative adaptive cruise control on traffic-flow characteristics," *IEEE Trans. Intell. Transp. Syst.*, vol. 7, no. 4, pp. 429–436, Dec. 2006.
[22] J. I. Ge and G. Orosz, "Dynamics of connected vehicle systems with delayed acceleration feedback," *Transp. Res. C, Emerging Technol.*, vol. 46, pp. 46–64, Sep. 2014.
[23] G. Orosz, "Connected cruise control: Modeling, delay effects, and nonlinear behavior," *Veh. Syst. Dyn.*, Jun. 2016. [Online]. Available: http://dx.doi.org/10.1080/00423114.2016.1193209
[24] G. Stépán, "Vibrations of machines subjected to digital force control," *Int. J. Solids Struct.*, vol. 38, no. 10, pp. 2149–2159, Mar. 2001.
[25] T. Insperger and G. Stépán, *Semi-Discretization for Time-Delay Systems: Stability and Engineering Applications*, ser. Applied Mathematical Sciences, vol. 178. Berlin, Germany: Springer-Verlag, 2011.

[26] D. Caveney, "Cooperative vehicular safety applications," *IEEE Control Syst. Mag.*, vol. 30, no. 4, pp. 38–53, Aug. 2010.
[27] S. Öncü, J. Ploeg, N. van de Wouw, and H. Nijmeijer, "Cooperative adaptive cruise control: Network-aware analysis of string stability," *IEEE Trans. Intell. Transp. Syst.*, vol. 15, no. 4, pp. 1527–1537, Aug. 2014.
[28] M. di Bernardo, A. Salvi, and S. Santini, "Distributed consensus strategy for platooning of vehicles in the presence of time varying heterogeneous communication delays," *IEEE Trans. Intell. Transp. Syst.*, vol. 16, no. 1, pp. 102–112, Feb. 2015.
[29] I. Kolmanovsky and T. Makenberg, "Stochastic stability of a class of nonlinear systems with randomly varying time-delay," in *Proc. Amer. Control Conf.*, 2000, pp. 4304–4308.
[30] P. Park, "A delay-dependent stability criterion for systems with uncertain time-invariant delays," *IEEE Trans. Autom. Control*, vol. 44, no. 4, pp. 876–877, Apr. 1999.
[31] H. Gao and T. Chen, "New results on stability of discrete-time systems with time-varying state delay," *IEEE Trans. Autom. Control*, vol. 52, no. 2, pp. 328–334, Feb. 2007.
[32] D. Yue, Y. Zhang, E. Tian, and C. Peng, "Delay-distribution-dependent exponential stability criteria for discrete-time recurrent neural networks with stochastic delay," *IEEE Trans. Neural Netw.*, vol. 19, no. 7, pp. 1299–1306, Jul. 2008.
[33] R. Krtolica, U. Ozguner, H. Chan, H. Goktas, J. Winkelman, and M. Liubakka, "Stability of linear feedback systems with random communication delays," in *Proc. Amer. Control Conf.*, 1991, pp. 2648–2653.
[34] M. M. Gomez, G. Orosz, and R. M. Murray, "Stability of discrete-time systems with stochastically delayed feedback," in *Proc. Eur. Control Conf.*, 2013, pp. 2609–2614.
[35] O. L. V. Costa and M. D. Fragoso, "Stability results for discrete-time linear systems with Markovian jumping parameters," *J. Math. Anal. Appl.*, vol. 179, no. 1, pp. 154–178, Oct. 1993.
[36] E. I. Verriest and W. Michiels, "Stability analysis of systems with stochastically varying delays," *Syst. Control Lett.*, vol. 58, pp. 783–791, 2009.
[37] A. Laub, *Matrix Analysis for Scientists and Engineers*. Philadelphia, PA, USA: SIAM, 2005.
[38] A. F. Karr, *Probability*. Berlin, Germany: Springer-Verlag, 1993.
[39] K. J. Åström, *Introduction to Stochastic Control Theory*. New York, NY, USA: Academic, 1970.
[40] Sequences of Random Variables and Their Convergence, Statlect. [Online]. Available: http://www.statlect.com/seqrnd1.htm
[41] R. Khasminskii, *Stochastic Stability of Differential Equations*, 2nd ed. Berlin, Germany: Springer-Verlag, 2012.
[42] L. Shaikhet, *Lyapunov Functionals and Stability of Stochastic Functional Differential Equations*. Berlin, Germany: Springer-Verlag, 2013.
[43] H. Kushner, *Introduction to Stochastic Control*. New York, NY, USA: Holt, Rinehart and Winston, 1971.
[44] "Safety pilot," Univ. Michigan Transp. Res. Inst., Ann Arbor, MI, USA, 2012. [Online]. Available: http://safetypilot.umtri.umich.edu/
[45] V. Gupta, A. F. Dana, J. P. Hespanha, R. M. Murray, and B. Hassibi, "Data transmission over networks for estimation and control," *IEEE Trans. Autom. Control*, vol. 54, no. 8, pp. 1807–1819, Aug. 2009.
[46] F. Bai and H. Krishnan, "Reliability analysis of DSRC wireless communication for vehicle safety applications," in *Proc. IEEE Intell. Transp. Syst. Conf.*, 2006, pp. 355–362.
[47] W. B. Qin and G. Orosz, "Digital effects and delays in connected vehicles: Linear stability and simulations," in *Proc. ASME Dyn. Syst. Control Conf.*, 2013, pp. 1–10, DSCC013-3830, V002T30A001.
[48] M. Wang, W. Daamen, S. P. Hoogendoorn, and B. van Arem, "Rolling horizon control framework for driver assistance systems. Part I: Mathematical formulation and non-cooperative systems," *Transp. Res. C, Emerging Technol.*, vol. 40, pp. 271–289, Mar. 2014.
[49] J. Guckenheimer and P. Holmes, *Nonlinear Oscillations, Dynamical Systems, and Bifurcations of Vector Fields*, vol. 42. Berlin, Germany: Springer-Verlag, 1983.
[50] D. Bachrathy and G. Stépán, "Bisection method in higher dimensions and the efficiency number," *Periodica Polytechnica*, vol. 56, no. 2, pp. 81–86, 2012.
[51] L. Zhang and G. Orosz, "Motif-based design for connected vehicle systems in presence of heterogeneous connectivity structures and time delays," *IEEE Trans. Intell. Transp. Syst.*, vol. 17, no. 6, pp. 1683–1651, Jun. 2016.
[52] W. Feller, *An Introduction to Probability Theory and Its Applications*, vol. 1. New York, NY, USA: Wiley, 1950.
[53] J. I. Ge and G. Orosz, "Optimal control of connected vehicle systems with communication delay and driver reaction time," *IEEE Trans. Intell. Transp. Syst.*, to be published.

Wubing B. Qin received the B.Eng. degree from Huazhong University of Science and Technology, Wuhan, China, in 2011. He is currently working toward the Ph.D. degree in mechanical engineering with University of Michigan, Ann Arbor, MI, USA.

His research interests include dynamics and control of connected vehicles and nonlinear and stochastic systems with time delays.

Marcella M. Gomez received the B.Sc. degree from University of California, Berkeley, CA, USA, in 2008 and the M.Sc. and Ph.D. degrees from California Institute of Technology, Pasadena, CA, USA, in 2011 and 2015, respectively, all in mechanical engineering.

She is a Postdoctoral Researcher with the Department of Electrical Engineering and Computer Science, University of California, Berkeley. Her research interests include control and dynamics of time delay systems with applications ranging from connected vehicles to genetic regulatory networks.

Gábor Orosz received the M.Sc. degree in engineering physics from Budapest University of Technology and Economics, Budapest, Hungary, in 2002 and the Ph.D. degree in engineering mathematics from University of Bristol, Bristol, U.K., in 2006.

He held postdoctoral positions with University of Exeter, Devon, U.K., and with University of California, Santa Barbara, CA, USA, before joining University of Michigan, Ann Arbor, MI, USA, in 2010 as an Assistant Professor in mechanical engineering. His research interests include nonlinear dynamics and control, time delay systems, and networks and complex systems with applications on connected and automated vehicles and biological networks.